



The contents of this report are not to be used for advertising, publication, or promotional purposes. Citation of trade names does not constitute an official endorsement or approval of the use of such commercial products.



PRINTED ON RECYCLED PAPER

# Laboratory Description of Harbor Idealized Tests

## Volume I: Main Text and Appendixes A Through C

by Michael J. Briggs, Edward F. Thompson  
Debra R. Green, Linda S. Lillycrop  
Coastal Engineering Research Center  
U.S. Army Corps of Engineers  
Waterways Experiment Station  
3909 Halls Ferry Road  
Vicksburg, MS 39180-6199

Accession For	
NTIS CRA&I	<input checked="" type="checkbox"/>
DTIC TAB	<input type="checkbox"/>
Unannounced	<input type="checkbox"/>
Justification .....	
By .....	
Distribution /	
Availability Codes	
Dist	Avail and/or Special
A-1	

Final report

Approved for public release; distribution is unlimited

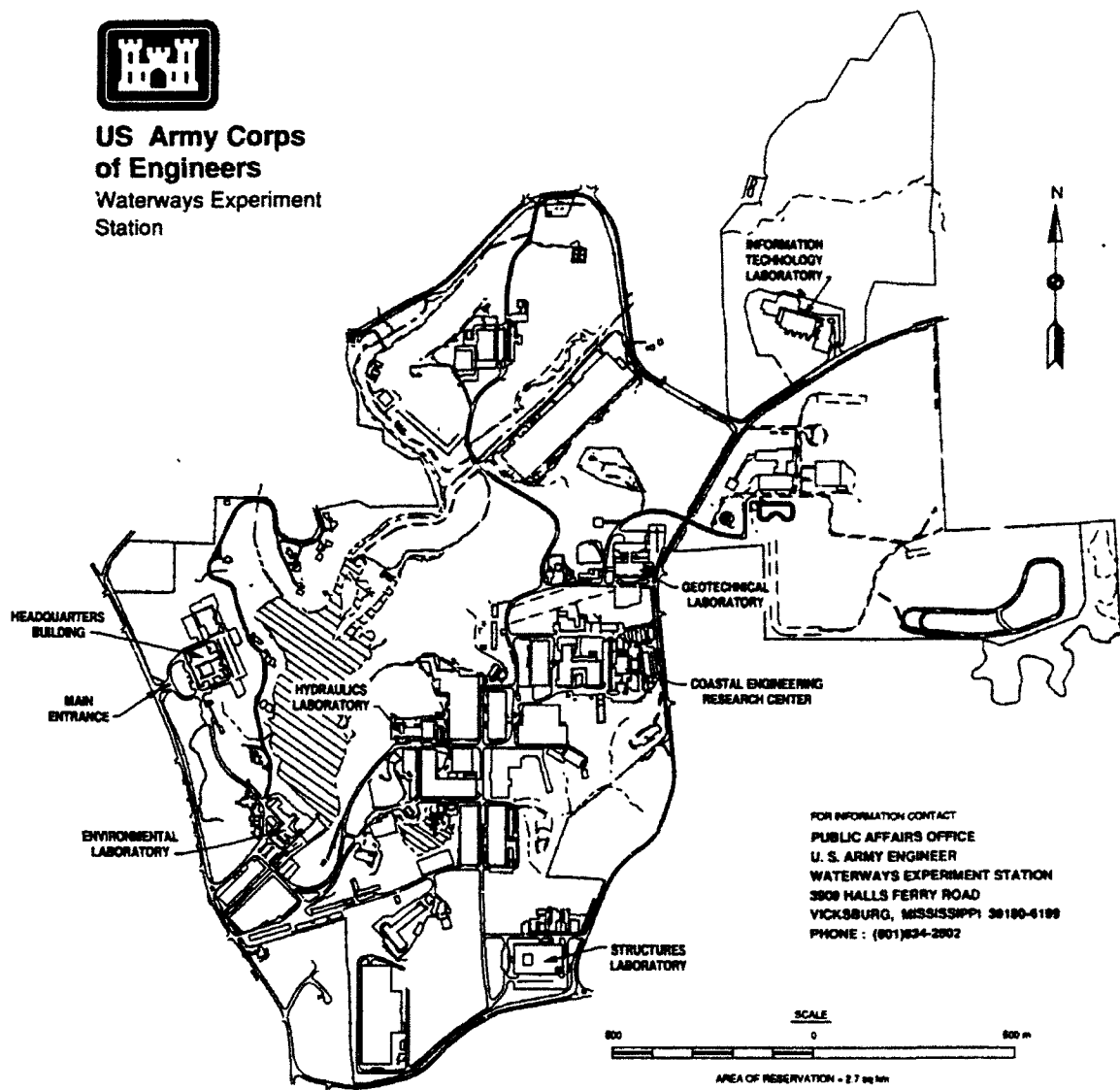
DTIC QUALITY INSPECTED 2

Prepared for U.S. Army Corps of Engineers  
Washington, DC 20314-1000

Under Work Units 31672 and 31592



**US Army Corps  
of Engineers**  
Waterways Experiment  
Station



**Waterways Experiment Station Cataloging-in-Publication Data**

Laboratory description of harbor idealized tests / by Michael J. Briggs ...  
[et al.], Coastal Engineering Research Center ; prepared for U.S. Army  
Corps of Engineers.

2 v. : ill. ; 28 cm. — (Technical report ; CERC-93-1)

Includes bibliographical references.

1. Harbors — Hydrodynamics — Simulation methods. 2. Hydraulic  
models. 3. Ocean waves — Mathematical models. 4. Shoaling (Hy-  
draulic engineering) I. Briggs, Michael Jeffrey. II. United States. Army.  
Corps of Engineers. III. Coastal Engineering Research Center (U.S.)  
IV. U.S. Army Engineer Waterways Experiment Station. V. Coastal En-  
gineering Research Program. VI. Series: Technical report (U.S. Army  
Engineer Waterways Experiment Station) ; CERC-93-1.

TA7 W34 no.CERC-93-1

# Contents

---

Preface . . . . .	iv
Conversion Factors, Non-SI to SI Units of Measurement . . . . .	v
1—Introduction . . . . .	1
Background and Purpose . . . . .	1
Report Organization . . . . .	4
2—Experimental Design . . . . .	6
Model Set-up . . . . .	6
Wave Conditions . . . . .	7
Test Program . . . . .	8
Testing Procedure . . . . .	19
Data Analyses . . . . .	23
Data Archival . . . . .	28
3—Results and Analysis . . . . .	29
Regular Waves . . . . .	29
Channel Entrance . . . . .	33
Harbor Resonance . . . . .	36
Wave Group . . . . .	41
Irregular Waves . . . . .	42
Wave-Current . . . . .	52
4—Summary and Conclusions . . . . .	58
References . . . . .	62
Appendix A: Notation . . . . .	A1
Appendix B: Test Case Run Numbers . . . . .	B1
Appendix C: Gage Coordinates . . . . .	C1
Appendix D: Wave Periods and Heights . . . . .	D1

# Preface

---

This report was authorized as part of the Civil Works Research and Development Program sponsored by Headquarters, U.S. Army Corps of Engineers (HQUSACE). It is a product of the Coastal Flooding and Storm Protection Program under "Laboratory Simulation of Nearshore Waves," Work Unit 31672, "Wave Estimation for Design," Work Unit 31592, and the Harbor Entrances and Coastal Channels Program under "Modeling Waves in Harbors," Work Unit 32486. Testing was conducted from July to October 1988, and data reduction and report preparation were completed in August 1992, at the U.S. Army Engineer Waterways Experiment Station's (WES's) Coastal Engineering Research Center (CERC). Messrs. John H. Lockhart, Jr., John G. Housley, David A. Roellig, and Barry W. Holliday were HQUSACE Technical Monitors for the Civil Works Research and Development Program. Program Manager of the Coastal R&D Program at CERC during testing was Dr. C. Linwood Vincent. Ms. Carolyn Holmes was Program Manager during report preparation.

This report was prepared by Mr. Michael J. Briggs, Wave Processes Branch (WPB), Wave Dynamics Division (WDD), Dr. Edward F. Thompson, Research Division (RD), Mrs. Debra R. Green, WPB, and Mrs. Linda S. Lillycrop, Prototype Measurement and Analysis Branch, Engineering Development Division, formerly with Oceanography Branch (OB), RD, under the direct supervision of Mr. Dennis G. Markle, Chief, WPB. General supervision was provided by Dr. Martin C. Miller, Chief, OB, Mr. C. E. Chatham, Jr., Chief, WDD, Mr. H. Lee Butler, Chief, RD, Mr. Charles C. Calhoun, Jr., Assistant Director, CERC, and Dr. James R. Houston, Director, CERC.

Numerous individuals contributed to the successful completion of this project. Mr. David A. Daily, WES Instrumentation Services Division, maintained the directional spectral wave generator, current meters and wave gages, and associated electronics. Mr. Larry A. Barnes, WPB, designed the model and interfaced with the WES shops. Mr. James M. Kaihatu, OB, participated in preliminary analysis and comparison of the wave-current data with numerical models.

Director of WES during publication of this report was Dr. Robert W. Whalin and Commander was COL Leonard G. Hassell, EN.

# Conversion Factors, Non-SI to SI Units of Measurement

---

Non-SI units of measurement used in this report can be converted to SI units as follows:

Multiply	By	To Obtain
cubic feet	0.02831685	cubic meters
degrees (angle)	0.01745329	radians
feet	0.3048	meters
gallons (U.S. liquid) per minute	3.785412	cubic decimeters per minute
inches	2.54	centimeters
knots (international)	0.5144444	meters per second
square feet	0.09290304	square meters

# 1 Introduction

---

## Background and Purpose

As waves travel into harbors from deep water, nonlinear processes transfer energy from the wind wave frequencies to long waves with periods on the order of several minutes and wavelengths much longer than the wind waves. If the periods of these long waves correspond with natural (resonant) periods of the harbor, strong harbor oscillations can be induced which can produce dangerous mooring conditions, structural damage, and sediment deposition or erosion within the harbor.

Harbor resonance (also known as seiche, surge, or resonant oscillations) is the phenomenon that occurs when the amplitude of oscillation increases until energy loss balances energy input. A harbor has certain preferential frequencies or periods at which it oscillates in a standing wave pattern. These frequencies or periods are a function of the harbor's geometrical configuration, dimensions, and water depth. The resonant mode with the longest period is the Helmholtz, or pumping, mode because the water appears to move up and down in unison throughout the harbor. Shorter period modes are characterized by an increasing number of nodes and antinodes within the harbor. Higher modes (i.e., higher frequency, lower period) are characterized by an increasing number of nodes and antinodes within the harbor. Water can oscillate in longitudinal, transverse, or diagonal directions for the different modes.

Energy sources for harbor resonance include these nonlinearly generated long waves, free long waves from distant sources, tsunamis, and atmospheric pressure disturbances (Okihiro and Seymour 1992). Often, long waves with periods greater than 25 sec (i.e., frequencies less than 0.04 Hz) are referred to as infragravity waves. Munk (1949) and Longuet-Higgins and Stewart (1962) suggested that surf beat, the reflection of free long waves in the surf zone, was a possible mechanism of harbor resonance. Bowers (1977) observed that setdown beneath wave groups can excite harbor oscillations if the group period is close to the natural period of the harbor. Many other researchers (Sand 1982, Kirkegaard and Nielsen 1982) have confirmed wave groups as a forcing mechanism for harbor resonance. Okihiro, Guza, and Seymour (1992) have shown that an increase

in infragravity energy and harbor resonance in Barbers Point, Oahu, Hawaii, harbor is highly correlated with an increase in wind wave and infragravity energy outside the harbor.

Moored vessels can experience resonant oscillation if their natural period in surge or sway corresponds to a harbor resonance mode and they are moored in the vicinity of the node. This excessive ship motion can prevent loading and unloading of the ship for a number of days. In some cases, extensive damage to the ship can result if the mooring lines fail. On February 8, 1988 a Coast Guard vessel was in the process of entering the MARISCO, Ltd. drydock in Barbers Point, Oahu, Hawaii, harbor when they both sustained damage due to harbor seiching under relatively calm conditions outside the harbor (Noda and Associates, Inc. 1988).

Harbor wave response can be estimated from field measurements, and physical and numerical models. Each of these three sources of information has assumptions and limitations that restrict its accuracy. The prototype measurements are used to calibrate both the physical and numerical models and verify wave response at selected locations within the harbor. However, they may be expensive to obtain, can only be collected after the harbor is built, and measured conditions may not correspond to the extreme conditions the harbor will experience. Numerical models are often used by themselves because of funding constraints. However, the user should recognize their limitations, which include (a) grid resolution, extent, and boundaries to adequately define the wave field, (b) linear wave theory assumptions, which do not include frequency and directional spreading of the wave field, and (c) proper selection of reflection and bottom boundary friction coefficients. When used in conjunction with physical models, numerical models can assist the physical model in the selection of test conditions; incident wave conditions having little effect on the harbor are not tested. The physical model provides an opportunity to test wave conditions that were not measured in the field, but are of interest from a design standpoint. The physical model data are also used to calibrate and verify the numerical model. Although physical models can accurately simulate linear and nonlinear phenomena (Elgar et al. 1992, Briggs and Smith 1990), they have limitations that include scale effects and control of reflections due to the finite extent of the model and possible spurious waves from the simulation of the wave field with a wave-maker. Thus, although each source of information has limitations that are not fully understood, when the methods are combined, a synergism is achieved that provides better engineering estimates of wave response in the design and modification of harbors.

A three-dimensional, physical model study of an idealized harbor and entrance channel using regular and irregular waves and tidal ebb currents was conducted in the directional spectral wave basin. The purpose of this study was to (a) gain a better understanding of the physics involved in wave transformation from deep water into harbors, (b) accurately reproduce this transformation in the physical model, (c) verify the HARBD numerical model (Chen, 1984 and 1986; Chen and Mei 1974), a steady-state

finite element model that includes the effects of bottom friction and boundary absorption in harbors of arbitrary configuration and variable bathymetry, and (d) generate a data set for improving Corps design procedures.

Preliminary comparisons of the low-reflective phase of the regular series data with HARBD were made by Lillycrop, Thompson, and Briggs (1991). Agreement was good in the entrance channel, but comparisons were inconsistent inside the harbor. These results are similar to those found by Crawford and Chen (1988) in comparing HARBD with a physical model of the small-boat harbor at Barcelona, New York. Explanations of this discrepancy included inadequate resolution of the numerical grid, refinement of the reflection and bottom friction coefficients, and possible effects of wave transformation between the wavemaker and the numerical model offshore boundary. These preliminary comparisons between the two models is encouraging, but future study is required, especially on the sensitivity of the reflection and bottom coefficients.

The harbor idealized tests included a 1:45 (i.e., 45 ft<sup>1</sup> in the prototype equals 1 ft in the model) scale physical model of a rectangular, 40-ft-deep flat-bottom harbor, contoured 40-ft entrance channel, and nearshore bathymetry. The bathymetry of the entrance channel and offshore area were retained from an existing physical model of Yaquina Bay, Oregon, to minimize construction costs.

Wave conditions included regular (monochromatic) and irregular (spectral) waves. Five test series consisting of (a) regular waves, (b) irregular waves with narrow and broad frequency and directional spreading, (c) harbor resonance, (d) wave group, and (e) channel entrance were created. The objectives of each test series are listed below:

- a. The regular wave series was designed to collect data in the physical model for comparison with the numerical model HARBD, which uses regular waves as input.
- b. The irregular wave series was created to study the effects of frequency and directional spreading and nonlinear wave-wave interactions on the harbor response.
- c. Free long waves, with wave periods corresponding to first and second modes along the longitudinal and transverse axes, were tested in the harbor resonance series to see how accurately theoretical resonant modes were reproduced in the physical and numerical models.

---

<sup>1</sup> A table of factors for converting non-SI units of measurement to SI units is presented on page v.

- d. A wave group series was created by combining a pair of regular waves with nearly the same wind wave frequencies. These frequencies were selected so that the difference between them matched an expected resonant frequency of the harbor and the evolution from a grouped incident wave train to a long-period harbor oscillation could be studied.
- e. In the channel entrance series, short-duration, reflection-free measurements were made in the entrance channel using regular waves to verify another numerical model.

Each of these test series was run with the physical model in a low-reflective and a reflective phase, by removing the energy-absorbing stone around the vertical wall perimeter of the harbor.

Finally, an ebb current was created to study wave-current interaction seaward of the entrance channel for the low-reflecting harbor boundaries. Data were collected for only the regular and irregular wave series for wave only, current only, and wave and current conditions. Kaihatu and Berry (1989) performed preliminary analysis of the regular wave series. They found wave heights were affected by the ebb current and refraction across the channel. Additional verification with numerical models developed by the U.S. Army Engineer Waterways Experiment Station (WES) Coastal Engineering Research Center (CERC) was recommended.

This data set is being used with other laboratory and numerical model data to provide insight into the complicated wave transformation mechanisms that influence harbors. Design guidance is being published in the form of technical notes, papers, and reports. In particular, the Barbers Point, Oahu, Hawaii, study (Briggs and Boc 1991; Briggs, Lillycrop, and McGehee 1992; Lillycrop and Briggs 1992) has benefitted from this data set relative to the effects of frequency and directional spreading and nonlinear energy transfer among wave components. Wave-current interaction data will be supplemented with the Cornell study of the effect of ebb currents flowing through an idealized inlet on regular waves (Briggs and Green 1992).

## Report Organization

This report describes the laboratory data collection effort. Chapter 2 of this report describes the experimental design including the model setup, wave conditions, test program, and testing procedure. Typical prototype wave periods were 8 and 14 sec (1.19- and 2.09-sec, respectively, in the model). A prototype wave height of 3.75 ft (1-in. model) was selected for all tests to prevent overtopping and breaking and minimize nonlinear interactions. Waves had overall mean wave directions of 0 deg and  $\pm 22.5$  deg, relative to a direction perpendicular to the wavemaker. Tidal ebb currents of 0.5 knot (0.88 fps prototype, 0.13 fps model) were created to study the

wave-current interaction in the nearshore region outside the entrance channel. Boundary conditions in the harbor and channel included fully reflecting vertical walls and low-reflecting, 1:1.3 revetted stone slopes. A total of 374 runs were completed using 20 capacitance wave gages and 4 electromagnetic current meters in 9 different gage configurations in the harbor corners and the entrance channel. Wave and current data were analyzed in the time domain using zero-downcrossing and in the frequency domain with spectral methods. Predicted and measured reflection coefficients were also provided to the numerical model.

Chapter 3 presents some examples of the analyses performed for each of the test series for the low-reflective phase. Wave-current phase data are also presented and discussed. Finally, Chapter 4 contains a summary of results and recommendations for future research. Appendix A is a notation of symbols and abbreviations used in this report, Appendix B is a listing of the test case run numbers, and Appendix C lists the gage coordinates. Appendix D (published under separate cover as Volume II) is a listing of wave periods and heights.

## 2 Experimental Design

---

### Model Setup

A three-dimensional, physical model of a rectangular harbor, entrance channel, and nearshore bathymetry was constructed in CERC's directional spectral wave generator (DSWG) basin. The harbor plan is a rectangle with a straight entrance channel. Although the plan is idealized, it was designed to resemble Barbers Point Harbor. The tests proved helpful in conducting a subsequent extensive series of tests with Barbers Point Harbor. The existing entrance channel and nearshore contours from the Yaquina Bay, Oregon, jetty stability study were utilized to minimize construction costs. A 1:45 length scale (i.e., 1:6.71 time scale) was selected because it was satisfactory for the wave conditions desired and had been used on the Yaquina Bay jetty study. Offshore contours extended to a depth of 68 ft (1.51-ft model). The depth of the harbor and entrance channel were 40 ft (0.89-ft model), although the channel had some deeper spots.

Figure 1 is a schematic of the basin layout. It shows coordinate values, lengths, bearings, angles, and beach slopes. The right-hand, global coordinate system origin is in the lower left corner of the basin. Auxiliary coordinate systems include the physical model  $X'/Y'$ <sup>1</sup> system with origin at paddle 1 and the numerical model  $X''/Y''$  system at the upper left-hand corner of the basin. The north arrow shown is for illustration purposes only. In the Yaquina Bay jetty stability tests, north was roughly parallel with the longitudinal harbor walls. The north jetty is the one on the left, closest to the DSWG. In addition to a 1:6 stone beach, the perimeter was lined with passive wave absorbers, comprised of metal frames covered with rubberized horsehair.

---

<sup>1</sup> For convenience, symbols and abbreviations are listed in the Notation (Appendix A).

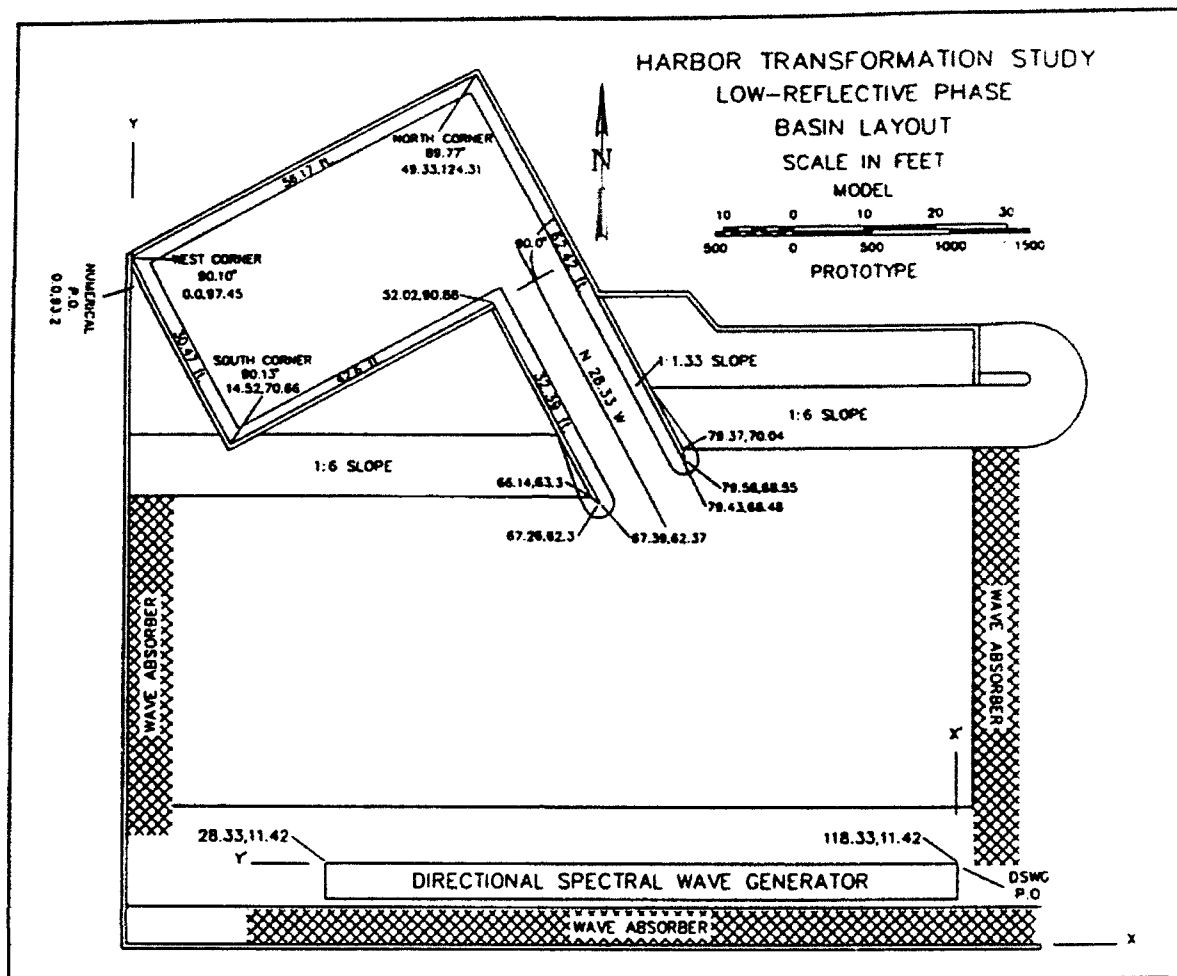


Figure 1. Basin layout

## Wave Conditions

Twenty-five wave conditions in five test series were created and tested. They consisted of (a) regular waves, (b) irregular waves, (c) harbor resonance, (d) wave group, and (e) channel entrance. In the regular wave series, wave period and direction were varied. In the irregular wave series, the effects of frequency and directional spreading were studied with narrow and broad unidirectional spectra and broad directional spectra. Harbor resonance was investigated using wave periods corresponding to first and second basin modes along the longitudinal and transverse axes. Wave grouping was studied by combining a pair of regular waves with nearly the same wind wave frequencies. These frequencies were selected so that the difference between them matched an expected resonant frequency of the harbor. Finally, the channel entrance series was a repeat of the regular wave series to ensure short-duration, reflection-free measurements in the entrance channel. A long-duration software ramp was included to permit the immediate measurement of the wave profile prior to contamination from basin reflections.

Table 1 lists the wave periods  $T$ , wave height  $H$ , overall mean wave direction  $\bar{\theta}$ , frequency spectrum peak enhancement factor  $\gamma$ , and directional spreading  $\sigma_m$  for each wave case. Typical prototype wave periods, in all series except harbor resonance and wave grouping, were 8.0 and 14.0 sec (1.19 and 2.09 sec model). In the harbor resonance series, prototype wave periods ranged from 34 to 119 sec (5.10 to 17.70 sec model). In the wave group series, prototype period combinations ranged from 6.71/7.45 to 13.42/16.84 sec (1.00/1.11 and 2.00/2.51 sec model).

The wave heights shown in Table 1 are based on the time domain, average zero downcrossing wave height  $\bar{H}_d$  for all but the irregular wave series. The frequency domain, zero-moment wave height  $H_{m0}$  was used for the irregular waves. Prototype wave heights as large as 18.75 ft (5-in. model) were originally created. They were iteratively corrected in a calibration phase using a gain factor (not shown) to reduce the wave height to a uniform 3.75 ft (1-in. model) for all tests to prevent overtopping and nonlinear interactions.

Overall mean wave directions were perpendicular to the DSWG (i.e.,  $\bar{\theta} = 0$  deg) for most of the test conditions. Angles of  $\bar{\theta} = \pm 22.5$  deg were included to study the effect of wave direction. Positive angles are measured clockwise from the perpendicular to the DSWG. A wave direction of  $\bar{\theta} = -22.5$  deg corresponds to a wave travelling parallel to the entrance channel.

Frequency spreading for the spectral cases in the irregular wave series ranged from  $\gamma = 3.3$  to  $\gamma = 7.0$ . Likewise, directional spreading ranged from unidirectional with  $\sigma_m = 1.0$  deg to broad directional with  $\sigma_m = 30.0$  deg.

## Test Program

The test program was divided into four phases: (a) calibration, (b) reflective, (c) low-reflective, and (d) wave-current. A total of 374 runs were made between 1 July and 5 October 1988 in all four phases. Table 2 summarizes the total number of runs for each wave condition in each phase. Appendix B contains individual run numbers for each phase by test case and gage layout. This appendix has one table for each of the first three phases and two tables for the wave-current phase. The first table for the wave-current phase gives the run numbers for the wave gages and the second gives the run numbers for the current meters.

### Calibration phase

The purpose of the calibration phase was to verify and correct the control signals as necessary to ensure the desired wave conditions. The harbor and entrance channel were lined with vertical, concrete block walls.

<b>Table 1 Target Wave Conditions</b>					
<b>Wave Case</b>	<b>T, sec</b>	<b>H, in.</b>	<b><math>\bar{\theta}</math>, deg</b>	<b><math>\gamma</math></b>	<b><math>\sigma_m</math>, deg</b>
<b>Regular Waves</b>					
A02	1.19	1	0	—	—
A03	2.09	1	0	—	—
A05	1.19	1	-22.5	—	—
A06	2.09	1	-22.5	—	—
A07	1.19	1	22.5	—	—
A08	2.09	1	22.5	—	—
<b>Irregular Waves</b>					
B01	1.19	1	0	3.3	1
B02	2.09	1	0	3.3	1
C01	1.19	1	0	7.0	1
C02	2.09	1	0	7.0	1
D01	1.19	1	0	3.3	30
D02	2.09	1	0	3.3	30
<b>Harbor Resonance</b>					
E21	5.10	1	0	—	—
E22	9.00	1	0	—	—
E23	9.90	1	0	—	—
E24	17.70	1	0	—	—
<b>Wave Group</b>					
F25	1.00/1.11	1	0	—	—
F26	2.00/2.51	1	0	—	—
F27	1.00/1.06	1	0	—	—
<b>Channel Entrance</b>					
G02	1.19	1	0	—	—
G03	2.09	1	0	—	—
G05	1.19	1	-22.5	—	—
G06	2.09	1	-22.5	—	—
G07	1.19	1	22.5	—	—
G08	2.09	1	22.5	—	—

**Table 2  
Test Program Summary**

Wall Cond.	Gage Type	No. Gages	Gage Layout	Wave Condition							Total
				A	B	C	D	E	F	G	
<b>Calibration Phase</b>											
R	WG	8	1	10	0	0	0	4	4	0	18
			2	17	0	0	0	4	4	0	25
			3	0	4	4	4	0	0	0	12
<b>Total</b>											55
<b>Reflective Phase</b>											
R	WG	20	1	8	2	2	2	4	4	6	28
			2	6	2	2	2	4	3	6	25
			3	6	2	2	2	4	3	0	19
			4	6	2	2	2	4	3	0	19
			5	6	2	2	2	4	3	0	19
<b>Total</b>											110
<b>Low-Reflective Phase</b>											
LR	WG	20	1	6	2	2	2	4	3	6	25
			2	6	2	2	2	4	3	6	25
			3	6	2	2	2	4	3	0	19
			4	6	2	2	2	4	3	0	19
			5	6	2	2	2	4	3	0	19
<b>Total</b>											107
<b>Wave-Current Phase</b>											
<b>Wave Only</b>											
LR	WG	20	1	6	2	2	2	0	0	0	12
<b>Current Only</b>											
LR	CM	3-4	2		6						6
<b>Wave-Current</b>											
	WG	20	1	6	2	2	2	0	0	0	12
LR	CM	3-4	2	36	12	12	12	0	0	0	72
<b>Total</b>											102
<b>Note: R = Reflective condition; LR = Low-reflective condition; WG = Capacitance wave gage; CM = Current meter, Marsh McBirney.</b>											

These walls were lined with a thin veneer of mortar to minimize irregularities along the inner face of the walls.

A total of 55 runs, using 8 capacitance wave gages in three gage layouts, were completed in this phase. Figures 2a to 2c show the relative gage positions in each of the three layouts, respectively. Table C1 in Appendix C lists X and Y gage coordinates in the global system for the calibration phase. Table C3 in Appendix C contains the corresponding gage coordinates in the X"/Y" numerical model coordinate system. The coordinate transformation between the two coordinate systems is given by

$$X'' = y_1 - Y \quad (1)$$

$$Y'' = X$$

where  $y_1$ , the distance along the y-axis between origins, is equal to 93.2 ft.

Gages 1, 3, and 8 were used for reflection analysis (see Data Analysis) of the 1:6 beach and remained in the same positions for all three layouts. Gage 1 was 8 ft in front of the DSWG, and 22.5 ft from the end (i.e., between the 3<sup>rd</sup> and 4<sup>th</sup> modules). The spacings between gages,  $x_{13} = 2$  ft and  $x_{18} = 7$  ft, were selected based on a compromise among the desired wavelength  $L$  and the respective optimum spacings  $\Delta l$  which satisfy

$$0.05L \leq \Delta l \leq 0.45L \quad (2)$$

The range of  $L$  which satisfies this equation is between 4.4 and 140.0 ft for both gage spacings.

A linear array, patterned after the CERC Field Research Facility array, with a unit lag spacing of 2 ft, was designed using gages 2-4-5-6-7 in layout 1. The period and frequency limits corresponding to these gage spacings were 0.67 to 4 sec and 0.25 to 1.5 Hz, respectively. Gages 4-5-6-7 were in the same positions in layout 3. In layout 2, these gages were moved to calibrate wave conditions inside the harbor.

### Reflective phase

After the calibration phase, a total of 110 runs were made in this first production phase of testing. Harbor and entrance channel walls remained in their reflective condition. Twenty capacitance wave gages in five gage layouts were used to densely sample wave conditions in the harbor and entrance channel. Figures 3a to 3e show the relative gage positions for the five layouts, respectively. The global and numerical model gage coordinates for this phase are also listed in Appendix C on Tables C1 and C3, respectively.

Incident conditions were recorded by gages 1 and 2 for all layouts. Gage 1 was 10 ft in front of the DSWG along its center line (i.e., between

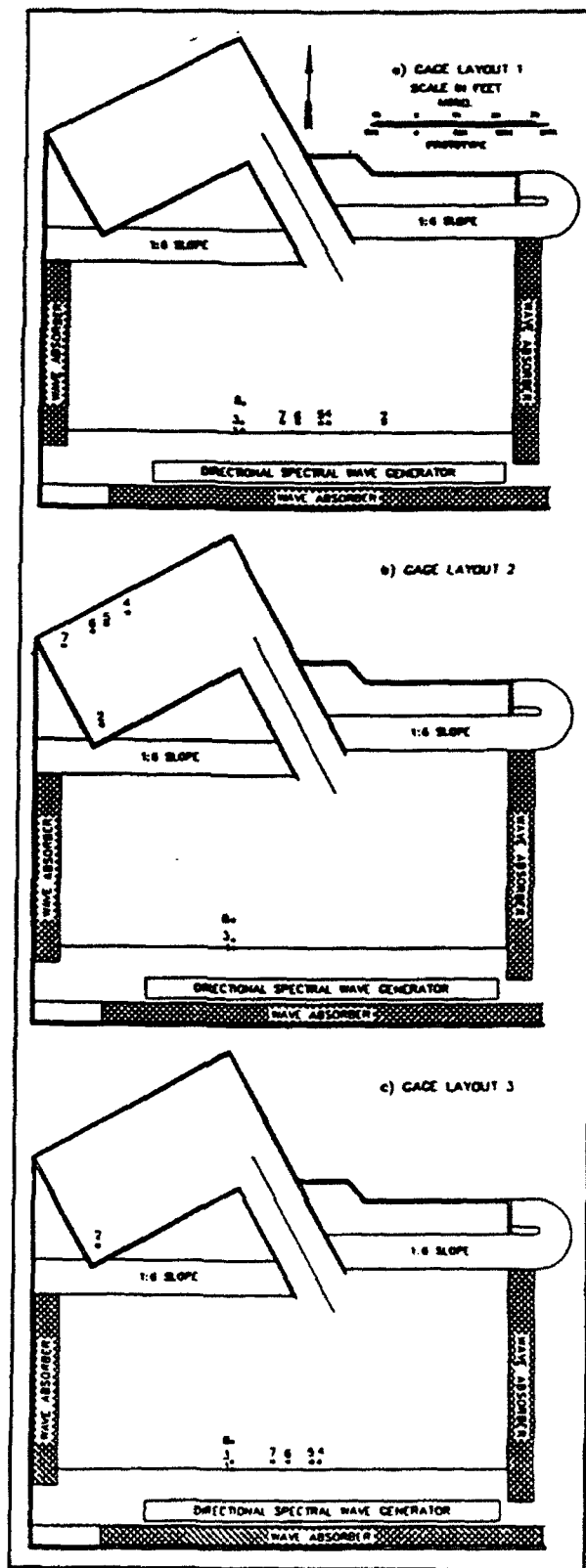


Figure 2. Calibration phase, gage layouts 1 to 3

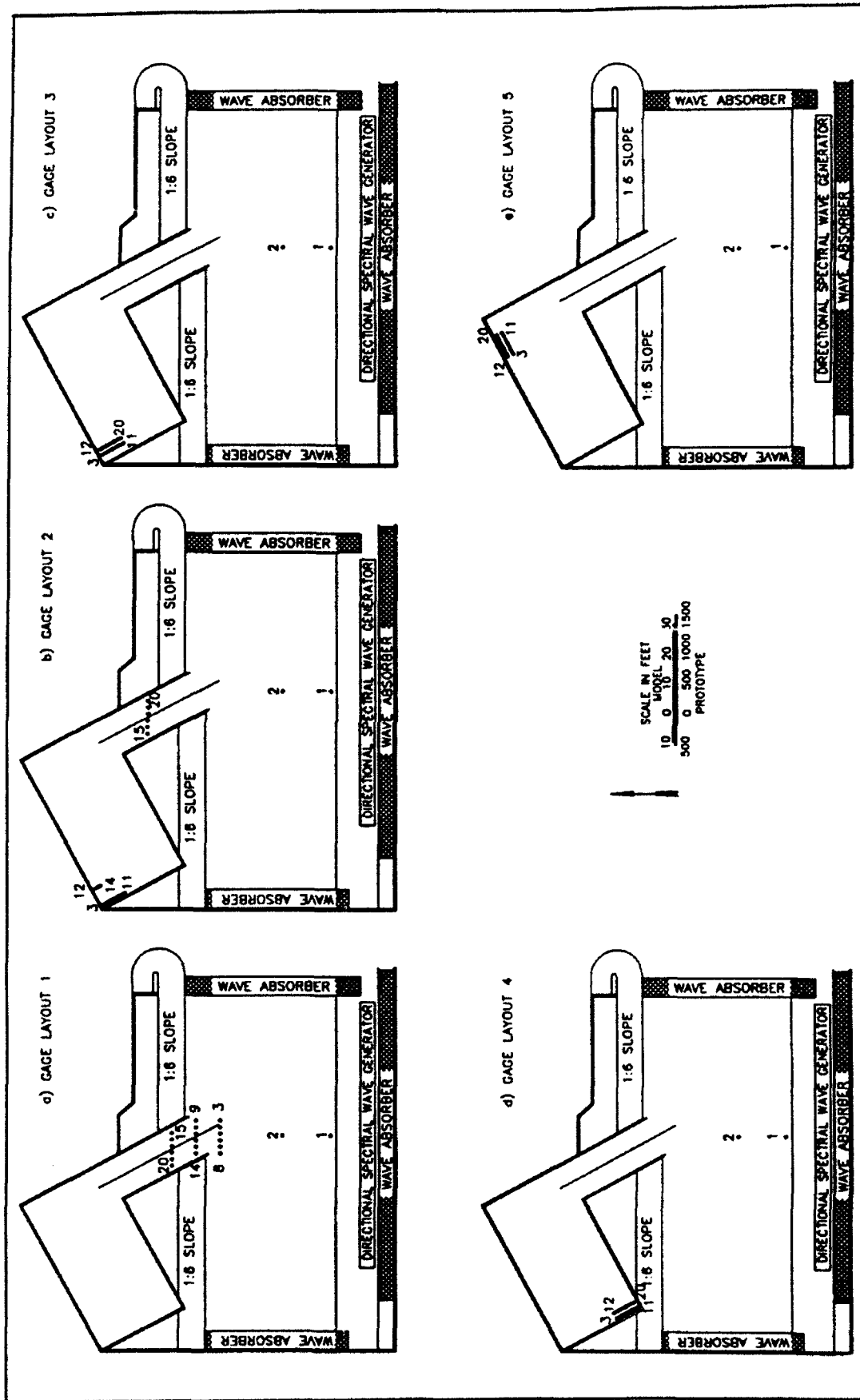


Figure 3. Reflective phase, gage layouts 1 to 5

modules 2 and 3, 45 ft from each end) in a water depth of approximately 1.11 ft (50 ft prototype). The DSWG was located so that its center line lined up with the intersection of the entrance channel center line and the line connecting the north and south jetty heads. Gage 2 was 26 ft from the DSWG, along this center line, in approximately the 0.89-ft (40 ft prototype) water depth.

In layout 1 (Figure 3a), gages 3 to 20 were aligned in a symmetrical array in the entrance channel. All gages were of the 0.89-ft depth (40 ft prototype), except for gages 7 and 8. Water depths for gages 7 and 8 were approximately 0.71 and 0.62 ft (32 and 28 ft prototype), respectively. Gages 15 to 20 were parallel to the DSWG and 12 ft farther along a line parallel to the y-axis from the tip of the north jetty. The spacing between gages in the x-direction was 2.2 ft. Gages 15 and 20 were also 2.2 ft from the vertical face of the channel walls on each side. The y-axis distance between gages 9 to 14 and 15 to 20 was 8 ft. Individual gage spacing was the same 2.2 ft. The lines connecting gages 9 and 15, 10 and 16, 11 and 17, etc., had the same bearing as the entrance channel. The y-axis distance between gages 3 to 8 and gages 9 to 14 was also 8 ft. The individual gage spacing was the same. The lines connecting gages 3 and 9, 4 and 10, 5 and 11, etc., were parallel to the y-axis.

Harbor response in corners and close to model boundaries is difficult to reproduce in numerical models. Therefore, gages were positioned in the harbor to give good resolution in these areas. In layout 2 (Figure 3b), gages 3 to 14 were located in the west corner of the harbor. Typical spacing between gages was 1 ft. Gage 3 was positioned 1 ft from both the north and west walls, measured perpendicular to each wall. Gages 12 to 14 were aligned parallel to gages 3 to 11 and 6 ft apart, measured perpendicular to the west wall. Gage 12 was also 1 ft from the north wall. Gages 15 to 20 were located in the entrance channel. They were 20 ft along a line parallel to the y-axis from the north jetty tip, parallel to the x-axis, and spaced 2.2 ft apart.

In layout 3 (Figure 3c), gages 3 to 11 and 12 to 20 were aligned as in layout 2, parallel to the west harbor wall. These two arrays fit inside the 6-ft space between the arrays in layout 2. The gage spacing was 1 ft. Gage 3 was 1 ft from the north wall of the harbor and 3 ft from the west wall, measured perpendicular to each wall. Gage 12 was 2 ft from gage 3, to allow room for the gage frame.

In gage layout 4 (Figure 3d), gages 3 to 20 were in the south corner of the harbor. Gages 3 to 11 were in one array and gages 12 to 20 in another spaced 2 ft apart, both parallel to the west harbor wall. Spacing between gages was 1 ft. Gage 11 was in the south corner, 1 ft from both the south and west walls. Gage 20 was 1 ft from the south wall and 3 ft from the west wall, measured perpendicular to each wall.

The final gage layout (Figure 3e) for the reflective phase was located in the north corner of the harbor. Gages 3 to 11 and 12 to 20 were located

parallel to the north wall with 1-ft spacing between gages. Gages 11 and 20 were on the extension of the entrance channel center line, 6.8 ft from the east wall. Gages 12 to 20 were 1 ft perpendicular from the north wall and gages 3 to 11 were 3 ft.

### **Low-reflective phase**

The next series of tests was the low-reflective phase. The harbor and entrance channel walls were lined with stone and the same wave conditions and gage layouts were used. A total of 107 runs were made. Figures 4a to 4e illustrate the relative gage positions for each of the five layouts, respectively. This figure is identical to Figures 3a to 3e, except that the boundaries are shown with stone revetment in place around the perimeter of the harbor and entrance channel. The global and numerical model gage coordinates for these layouts are listed in Appendix C in Tables C2 and C4, respectively.

The toe of the stone revetment was 2 ft out from the walls, corresponding to a slope of 1:1.3. In layouts 2 through 5, the initial distance out from the walls was increased from 1 ft to 3 ft, to put the gages the same distance from the toe of the stone slopes as they had been from the vertical wall in the reflective phase. This was felt to be a good compromise in keeping the distance as close to the walls as possible without having the waves experience any shoaling due to the slope. The individual gage spacing remained at 1 ft.

Gages 1 and 2 were again used to measure incident wave conditions. In layout 2, gages 15 to 20 in the entrance channel maintained the same spacing of 2.2 ft as before.

### **Wave-current phase**

The last series of tests was the wave-current phase. This was the first attempt to collect wave-current data in a three-dimensional laboratory experiment. The low-reflecting walls remained in the harbor and entrance channel. A 600-gpm pump was used to generate a steady ebb current with inflow located in the west corner of the harbor. A total of 102 runs (i.e., 24 with wave gages and 78 with current meters) were made in this phase.

Two new gage layouts in the nearshore region, seaward of the entrance channel, were selected for testing. The first layout, shown in Figure 5a, was for the 20 wave gages. Figure 5b shows the second layout for the four Marsh McBirney electromagnetic current meters. Since only two to four current meters worked at any one time, the tests were repeated six times to collect data at the 20 gage locations for both current only and wave-current interaction. The main difference between layouts was the reversal of the gage numbers in row 3, gages 16 to 20. The global and

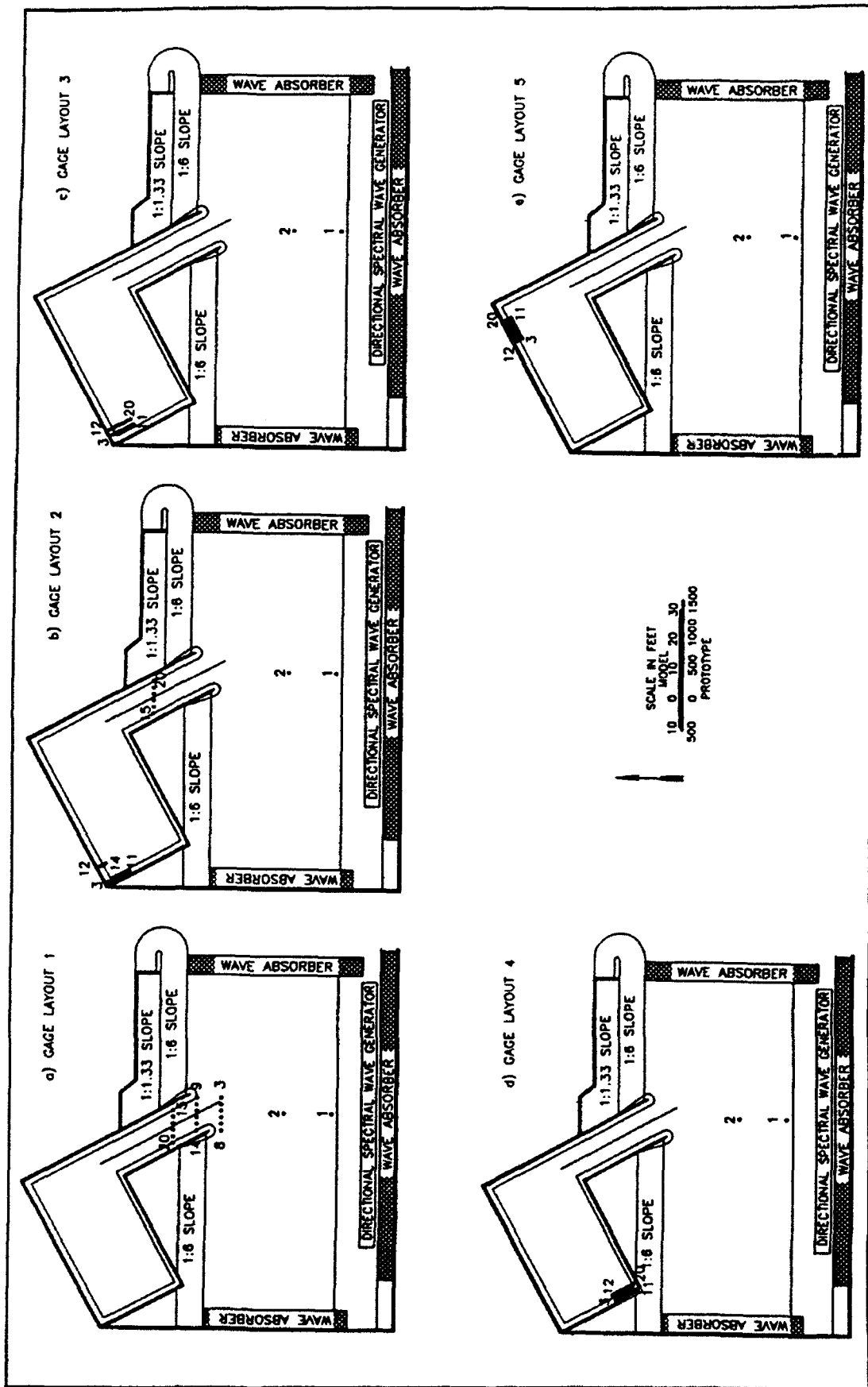


Figure 4. Low-reflective phase. gage layouts 1 to 5

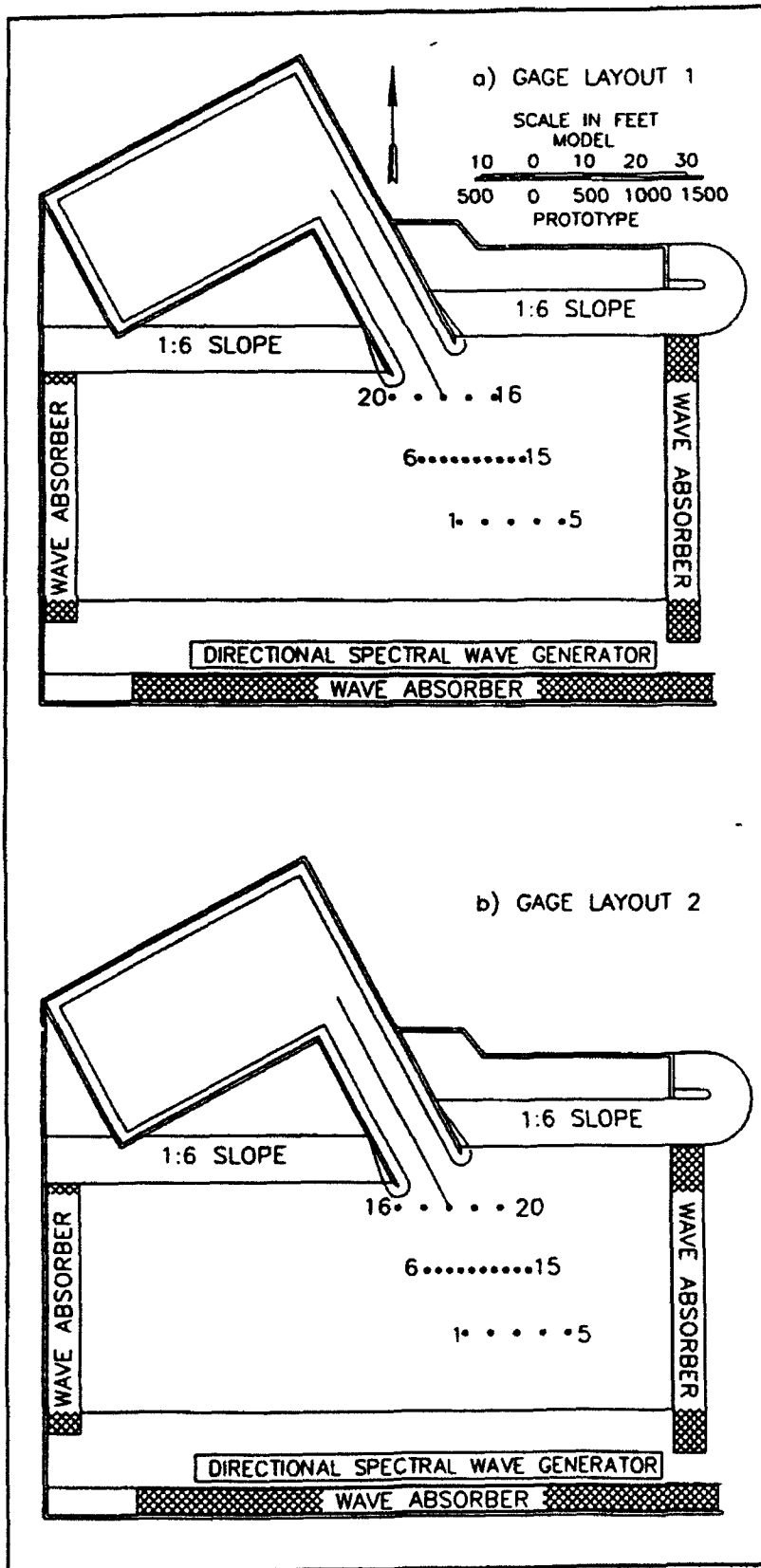


Figure 5. Wave-current phase, gage layouts 1 and 2

numerical model gage coordinates for these layouts are also listed in Appendix C in Tables C2 and C4, respectively.

The spacing between gages in both layouts was 5 ft for the end rows and 2.2 ft for the middle row. The first row was 23.25 ft in front of the DSWG. The spacing between rows 1 and 2 and rows 2 and 3 was 12 ft. Row 3 was approximately 4 ft from the tip of the north jetty and 10 ft from the tip of the south jetty. Gages 3, 11, and 18 were on the projected center line of the entrance channel.

Water depths for all gages inside the limits of the dredged channel were 0.89 ft (40-ft prototype). Depths for gages on the edges varied depending on location. Approximate water depths for these gages in layout 1 are listed below. The gage numbers in parentheses are for the current meters in layout 2.

Row No.	Gage No.	Depth, ft	
		Model	Prototype
1	1	0.89	40.0
	5	0.84	38.0
2	6	0.80	36.0
	7	0.80	36.0
	8	0.80	36.0
	14	0.71	32.0
	15	0.67	30.0
3	16(20)	0.80	36.0
	20(16)	0.62	28.0

The inlet for the pump was located in the 4-ft-deep sump in the south corner of the DSWG basin. It was submerged just above the bottom to minimize the creation of a circulation pattern due to the water intake. A steady current of approximately  $u_c = 0.13$  fps (5 knots or 0.88 fps prototype) was generated with the pump operating at full capacity. This value is based on a cross-sectional trapezoidal shape of the entrance channel of 13.5 ft at the surface and 9.5 ft at the bottom (due to the 2-ft-wide toe of the stone slopes). For the model depth of 0.89 ft, the cross-sectional area is 10.22 sq ft. The flow rate for the 600-gpm pump corresponds to 1.34 cu ft/sec.

The strength of this steady current relative to the wave celerity  $C$  and maximum horizontal water particle velocity at the surface  $u_{max}$  in the 40-ft-deep channel is listed below for the two wave periods  $T$  tested in

this phase. Numbers in parentheses are the corresponding prototype values. These ratios will change slightly for different water depths. A wave height of 3.75 ft (1-in. model) was assumed for the  $u_{max}$  calculation.

T, sec	C, fps	$u_{max}$ , fps	$u_c/C$	$u_c/u_{max}$
1.19 (8)	4.67 (31.3)	0.29 (1.9)	0.028	0.45
2.09 (14)	5.13 (34.4)	0.26 (1.7)	0.025	0.50

## Testing Procedure

### Control signal simulation and generation

The digital/analog rate for the DSWG is 20 Hz, corresponding to a time increment  $\Delta t = 0.05$  sec. Sixty-one time series (one for each paddle drive) were created for each wave condition. Table 3 lists the control signal lengths (in number of points and equivalent duration) and corresponding even frequency increments  $\Delta f$  between the lower and upper cutoff frequencies  $f_l = 0.05$  and  $f_u = 2.00$  Hz, respectively, for each test series.

The regular wave conditions in all test series were simulated by specifying the wave period(s)  $T$ , wave amplitude(s)  $a$ , and offset phase angle(s)  $\phi_y$ , controlling the wave direction  $\theta$  for each component(s). The height-to-stroke ratio, for computing the wavemaker stroke required to generate a given wave height, was calculated for each case.

The six spectral wave conditions in the irregular wave series were simulated in the frequency domain using a double summation, deterministic amplitude, random phase model (Borgman 1990; Briggs, Borgman, and Outlaw 1987). The directional spectra were simulated as the product of a

**Table 3**  
**Control Signal Generation Parameters**

Test Series	Control Signal Length		$\Delta f$ , Hz
	Pts	sec	
Regular	6,000	300	0.00333
Irregular	12,000	600	0.00667
Harbor Resonance	9,500	475	0.00211
Wave Group	9,500	475	0.00211
Channel Entrance	4,000	200	0.00200

Texel Marsden Arsloe (TMA) frequency spectra  $S_{TMA}(f)$  and a wrapped normal directional spreading function  $D(f, \theta)$ . The  $S_{TMA}(f)$  was calculated at 20 evenly spaced discrete frequencies, selected to give good resolution about the modal peak frequency  $f_p$ . Similarly, 16 discrete directions (i.e., 22.5 deg) were selected about  $\theta$  to give good resolution. Even frequency and direction increments were used to define the spectral energy about the peaks. Equivalent full width directional spread of 38 deg corresponds to the wrapped normal directional spread  $\sigma_m = 30$  deg used in the simulation.<sup>1</sup>

## Data collection

**Gage and water depth calibration.** The capacitance wave gages had 12-in.-long measurement rods. They were calibrated using the process IDCAL (calibration program for wave gages and current meters) over an 8-in. (0.67-ft) range each day prior to conducting tests. Table 4 lists the percentage of full-scale errors for each gage for each day of testing.

The Marsh McBirney current meters were borrowed from the WES Hydraulics Laboratory and had been calibrated in previous tests. Depth of immersion of the current meter sphere was 3.5 in. This distance corresponds to the distance between the center line of the sphere and the change in diameter of the stinger. The x and y axes of the current meters were aligned with the X'/Y' axes of the DSWG. One current meter ceased operations towards the end of tests in the wave-current phase, requiring a repeat of all 12 test conditions for gage location 14 (see Appendix B).

The water depth was maintained within  $\pm 0.001$  ft of the desired level by an automatic water level float control system.

**Data sampling.** Table 5 lists the data collection parameters for each of the five test series. Included for each are record length of data collected, corresponding number of points collected in a record, test duration, frequency increment, and gage layout. In the calibration phase, a shorter test duration was initially used in layout 1.

The CERC TAPEGAIN process (a procedure to run the wavemaker and collect data) is used to conduct the experiments. The user inputs the filename of the control signal, stored on a 9T magnetic tape, and a gain factor. The control signal is allowed to advance 10 sec (timed by a stop watch) to allow a common starting point for repeat tests. Then, the DSWG is turned on and a 10-sec hardware ramp is automatically activated to prevent damage to the DSWG in accelerating from no motion. The DSWG was not actually making waves until this instant in time. After the

---

<sup>1</sup> Unpublished data, March 1989, Jane M. Smith, Research Hydraulic Engineer, U.S. Army Engineer Waterways Experiment Station, Vicksburg, MS.



<b>Table 5 Data Collection Parameters</b>					
<b>Test Series</b>	<b>Record Length, sec</b>	<b>No. Points Record</b>	<b>Test Duration sec</b>	<b>Freq. Incr. Hz</b>	<b>Gage Layout</b>
<b>Calibration Phase</b>					
Regular	120	1,200	150	0.00833	1
	280 <sup>1</sup>	2,800	285	0.00357	2
Irregular	540	5,400	560	0.00185	3
Harbor Resonance	300	3,000	330	0.00333	1
	450	4,500	460	0.00222	2
Wave Group	240	2,400	270	0.00417	1
	450	4,500	460	0.00222	2
<b>All Other Phases</b>					
Regular	280	2,800	285	0.00357	All
Irregular	540	5,400	560	0.00185	All
Harbor Resonance	450	4,500	460	0.00222	All
Wave Group	450	4,500	460	0.00222	All
Channel Entrance	180	1,800	190	0.00556	All
<sup>1</sup> For test case HITA013 (i.e., case A01, run 3), only 120 sec of data were collected in gage layout 2.					

completion of this ramp at the beginning of the control signal (i.e., total delay of 20 sec), current meters or wave gages were sampled at 10 Hz (i.e., time increment  $\Delta t = 0.10$  sec). To minimize contamination from reflections in the channel entrance series, data were collected as soon as the waves left the DSWG.

**Current generation.** The procedure for generating the ebb current consisted of three steps. First, the pump was turned on to full flow. Next, 65 sec was allowed to elapse to enable the current to reach the array of gages closest to the DSWG (i.e., farthest from the current origin). Finally, the TAPEGAIN process was started. For the wave-current tests, two additional steps were added to the previous procedure. After an additional wait of 10 sec, the DSWG was started with the appropriate wave control signal.

## Data Analyses

Data analyses consisted of time domain zero-downcrossing, single channel frequency spectra, and Goda reflection. The Wave Dynamics Division TSAF (time series analysis computer program) package<sup>1</sup> was used. Also, visual observations were made of the circulation patterns produced by the currents.

### Zero-downcrossing analysis

Standard methods of zero-downcrossing analysis, as specified by the International Association of Hydraulic Research (IAHR (1986)), are incorporated in the TSAF software. Average wave period  $\bar{T}_d$ , significant wave period  $T_{H1/3,d}$ , and average of periods of the highest one-half of zero-downcrossing wave heights  $T_{H1/2,d}$  were calculated. Wave heights analyzed included maximum wave height  $H_{max}$ , significant wave height  $H_{1/3,d}$ , average zero-downcrossing wave height  $\bar{H}_d$ , and the minimum wave height  $H_{min}$ . Plots of cumulative probability distribution of extrema between crossings of the mean are generated.

### Single channel frequency spectral analysis

Data records were zero-measured, tapered by a 10-percent cosine bell window, Fourier transformed into the frequency domain, and band averaged between  $f_l = 0.01$  Hz and  $f_u = 2.00$  Hz. Table 6 lists the spectral analysis parameters for the different test series. Included in the table are the first point analyzed NFIRST, number of points in a record NTIME, record length  $T_r$  in sec, frequency increment  $\Delta f$  in Hz, resolution bandwidth  $B_e$  in Hz, number of frequencies analyzed between  $f_l$  and  $f_u$ , number of smoothed frequencies in each band, and degrees of freedom  $\nu$ . Since the energy in the regular cases is concentrated in the peak frequency, only one band was averaged in calculating  $B_e$ . For the spectral cases, a  $B_e = 0.0671$  Hz was selected to give an equivalent prototype  $B_e = 0.01$  Hz (i.e.,  $\sqrt{L_r}$  times 0.01 Hz). Spectral peak period based on the CERC method  $T_{p,c}$  and zero-moment wave height  $H_{m0}$  were calculated.

### Reflection analysis

The numerical model HARBD includes the effects of boundary absorption. Therefore, it is necessary to specify proper reflection coefficients

---

<sup>1</sup> Charles E. Long. 1986. "Laboratory wave generation and analysis: An instructional report for unidirectional wave generation and analysis," unpublished report, U.S. Army Engineer Waterways Experiment Station, Vicksburg, MS.

**Table 6  
Spectral Analysis Parameters**

Test Case	NFIRST	NTIME	T <sub>r</sub> , sec	Δf, Hz	B <sub>g</sub> , Hz	No. Frequencies		v
						Anal.	Smooth	
<b>Regular Waves</b>								
A02	2,400	400	40.0	0.0250	0.0250	80	1	2
A03	2,000	800	80.0	0.0125	0.0125	160	1	2
A05	2,400	400	40.0	0.0250	0.0250	80	1	2
A06	2,000	800	80.0	0.0125	0.0125	160	1	2
A07	2,400	400	40.0	0.0250	0.0250	80	1	2
A08	2,000	800	80.0	0.0125	0.0125	160	1	2
<b>Irregular Waves</b>								
B01	2,000	2,500	250.0	0.0040	0.0671	498	16	32
B02	1,000	4,400	440.0	0.0023	0.0671	876	29	58
C01	2,000	2,500	250.0	0.0040	0.0671	498	16	32
C02	1,000	4,400	440.0	0.0023	0.0671	876	29	58
D01	2,000	2,500	250.0	0.0040	0.0671	498	16	32
D02	1,000	4,400	440.0	0.0023	0.0671	876	29	58
<b>Harbor Resonance</b>								
E21	3,000	1,500	150.0	0.0067	0.0067	299	1	2
E22	2,000	2,500	250.0	0.0040	0.0040	498	1	2
E23	2,000	2,500	250.0	0.0040	0.0040	498	1	2
E24	1,500	3,000	300.0	0.0033	0.0033	597	1	2
<b>Wave Group</b>								
F25	2,500	2,000	200.0	0.0050	0.0050	398	1	2
F26	1,500	3,000	300.0	0.0033	0.0033	597	1	2
F27	2,500	2,000	200.0	0.0050	0.0050	398	1	2
<b>Channel Entrance</b>								
G02	1,000	400	40.0	0.0250	0.0250	80	1	2
G03	1,000	200	20.0	0.0500	0.0500	40	1	2
G05	1,000	400	40.0	0.0250	0.0250	80	1	2
G06	1,000	200	20.0	0.0500	0.0500	40	1	2
G07	1,000	400	40.0	0.0250	0.0250	80	1	2
G08	1,000	200	20.0	0.0500	0.0500	40	1	2

(i.e., ratio of reflected wave height to incident wave height) to accurately represent the boundary conditions. For the 1:6 beach slopes opposite the DSWG, measured reflection coefficients  $K_{r,m}$  from the physical model and predicted reflection coefficients  $K_{r,p}$  from Ahrens's (1987) work with rubble-mound reef breakwaters were calculated. For the 1:1.3 stone slopes lining the entrance channel and the harbor,  $K_{r,p}$  values only were provided.

The physical model reflection analysis is based on the work of Goda and Suzuki (1976) for separating the reflected and incident spectra using the time series from two gages. Three gages are used in the array to provide two different spacings for resolution of a wider range of frequencies. Reflected and incident spectra are averaged where they overlap, increasing the accuracy in this range. As mentioned earlier, the spacing between gages was selected to optimize the range of frequencies and wavelengths that could be resolved. It is necessary to have the shorter spacing first (i.e., offshore) to achieve the full benefit of the algorithm.

Table 7 lists the 1:6 beach slope  $K_{r,m}$  from the calibration phase for each wave case. The analysis parameters NFIRST and NTIME were the same as those listed in Table 6. One or more runs were made for each case with gain factors around the gains used in the calibration phase to ensure accurate reproduction of a 1-in. (0.083-ft) incident wave height. Final values of  $K_{r,m}$  were calculated by interpolating between the measured incident wave height and the corresponding gain factors (see Table 7).

Values of  $K_{r,p}$  calculated as a function of wavelength  $L_p$ , water depth  $h$ , and slope  $\theta$  are given by

$$K_{r,p} = \frac{1.0}{1.0 + 8.281 \left( \frac{l}{L_p} \right)^{0.951}} \quad (3)$$

where  $l = h \cot \theta$ . A model depth of 0.89 ft (40-ft prototype) was used for the 1:1.3 harbor and channel entrance. For the 1:6 beach slope, a depth of 0.95 ft (42.75-ft prototype) was used. Table 8 lists  $K_{r,p}$  for each wave case for both the 1:1.3 stone slopes and the 1:6 beach slopes. Interpolated values of  $K_{r,m}$  from Table 7 are also listed for comparison.

The measured reflection coefficients exceeded the predicted values except for the last three cases in the harbor resonance series. Goda's analysis assumes that incident and reflected waves travel parallel to the orientation of the two gages. Waves at an angle will probably produce erroneous results, the magnitude of which is not known. Therefore, the measured values are probably somewhat larger than actually present, and engineering judgement should be used in selecting values for use in numerical models.

**Table 7**  
**Measured Reflection Coefficients for 1:6 Beach Slopes**

Test Case	Run No.	Gain Factor	H <sub>mo</sub> , ft	K <sub>r,m</sub> , percent
<b>Regular Waves</b>				
A02	3	0.10	0.04855	19.47
	4	0.05	0.02117	24.72
A03	2	0.40	0.14830	25.49
	3	0.20	0.07363	34.65
A05	2	0.40	0.14840	24.66
	3	0.20	0.07337	31.61
A06	2	0.40	0.14840	36.43
	3	0.20	0.07695	38.68
A07	2	0.40	0.11510	29.44
	3	0.20	0.05017	53.62
A08	2	0.40	0.22190	29.62
	3	0.20	0.10410	28.30
<b>Irregular Waves</b>				
B01	1	1.00	0.06543	29.48
	2	0.92	0.05979	29.95
B02	1	1.20	0.07659	31.34
	2	1.14	0.07259	31.45
C01	1	1.00	0.07170	28.49
	2	0.92	0.06533	27.70
C02	1	1.20	0.07606	32.00
	2	1.20	0.07577	32.09
D01	1	1.00	0.05418	31.15
	2	1.44	0.07665	30.66
D02	1	1.20	0.05222	26.36
	2	1.88	0.08362	25.75
<b>Harbor Resonance</b>				
E21	2	0.30	0.12650	57.68
E22	2	0.50	0.13190	46.22
E23	2	0.50	0.09179	38.87
E24	2	1.00	0.12730	39.31
<b>Wave Group</b>				
F25	2	0.40	0.13030	54.51
F26	2	0.40	0.11640	47.23
F27	2	0.40	0.10280	68.95

**Table 8**  
**Predicted versus Measured Percent Reflection Coefficients**

Wave Case	Wave Period sec	Wavelength, ft		Predicted $K_{r,p}$ Stone Slope		Measured $K_{r,m}$ <sup>1</sup> Stone Slope
		1:1.3	1:6	1:1.3	1:6	1:6
<b>Regular Waves</b>						
A02	1.19	5.55	5.67	33	11	19
A03	2.09	10.72	11.04	49	18	27
A05	1.19	5.55	5.67	33	11	27
A06	2.09	10.72	11.04	49	18	37
A07	1.19	5.55	5.67	33	11	34
A08	2.09	10.72	11.04	49	18	29
<b>Irregular Waves</b>						
B01	1.19	5.55	5.67	33	11	30
B02	2.09	10.72	11.04	49	18	31
C01	1.19	5.55	5.67	33	11	28
C02	2.09	10.72	11.04	49	18	32
D01	1.19	5.55	5.67	33	11	31
D02	2.09	10.72	11.04	49	18	26
<b>Harbor Resonance</b>						
E21	5.10	27.09	27.98	70	35	58
E22	9.00	48.05	49.63	80	49	46
E23	9.90	52.87	54.62	82	51	39
E24	17.70	94.66	97.79	89	64	39
<b>Wave Group</b>						
F25	1.00/1.11	4.38/5.06	4.46/5.17	29/32	9/10	55
F26	2.00/2.51	10.22/13.04	10.52/13.45	48/54	18/21	47
F27	1.00/1.06	4.38/4.75	4.46/4.85	29/31	9/9	69

<sup>1</sup> Measured  $K_{r,m}$  are interpolated from values in Table 7.

## **Current test observations**

Visual observations of the flow patterns during the harbor resonance series revealed strong von Karman vortex sheets being generated at the tip of the north and south jetties. The longer wavelengths were more conducive to initiating this type of hydrodynamic response than the shorter wavelengths of the wind waves.

A qualitative look at the circulation patterns in the basin using dye tracers was performed on two occasions. Initially, the flow entering the model went across the harbor towards the channel entrance and out into the nearshore region. After several minutes a circulation was set up in the harbor. Tip vortices were generated at the jetties on initial start-up. The flow in the nearshore region did not appear to be strongly influenced by the intake to the pump. It followed the channel alignment towards the DSWG with a slight turning to the right. Once waves were introduced, some of the dye was washed back towards the beach due to the wave action.

## **Data Archival**

The data has been archived on 9T, magnetic tapes, in ASCII format for future analysis. The Virtual Memory System (VMS) "BACKUP" utility was used on these tapes. The data will also be archived on WORM disks for more durable storage. Color slides of some of the tests were also taken.

## 3 Results and Analysis

---

In this chapter, physical model results are presented. An example case from each of the five test series for the low-reflective phase (i.e., harbor walls revetted with stone) is discussed. A representative case from the wave-current phase (also with stone revetment) is also presented. Although no examples are presented for the calibration and reflective phases, these data are archived and contained in the appendices. Incident (offshore) and local wave conditions in the harbor or entrance channel are shown for each example.

### Regular Waves

The objective of the regular wave series was to collect data in the physical model for comparison with the state-of-the-art numerical model HARBD. Six hundred combinations of wave and gage location (i.e., 6 waves x 5 gage layouts x 20 gages per layout) were collected for both the reflective and low-reflective phases and made available for comparison with the numerical model. Gage 18 in layout 3 for case A08 (Run 11) was selected as an example. This gage is in the west corner of the harbor, where one might expect the greatest transformation effects, in a water depth of 40 ft (0.89-ft model). The incident waves were measured at gage 2, located on the flat bottom at a water depth of 68 ft (1.51-ft model).

Zero-downcrossing and spectral wave periods and heights, surface elevation time series, frequency spectra, and cumulative probability distributions for wave height are presented for the incident and interior gage locations. Table 9 lists measured zero-downcrossing periods  $\overline{T}_d$ ,  $T_{H1/3,d}$ , and  $T_{H1/2,d}$  and wave heights  $H_{max}$ ,  $H_{1/3,d}$ ,  $\overline{H}_d$ , and  $H_{min}$  for the incident and interior gages. Spectral peak period  $T_{p,c}$  and zero-moment wave height  $H_{m0}$  are also presented. For regular waves,  $H_{m0}$  is usually 1.4 (i.e.,  $\sqrt{2}$ ) times greater than  $\overline{H}_d$  for equivalent wave energy. A complete listing of measured wave periods and heights for the regular wave series is given in Appendix D. The nomenclature varies slightly because of limitations of the Lotus spreadsheet. The equivalent wave period and height symbols are listed on the first page of Appendix D.

Table 9 Measured Wave Periods and Heights for Regular Wave Series									
Gage No.	$\bar{T}_d$ sec	$T_{H1/3,d}$ sec	$T_{H1/2,d}$ sec	$T_{p,c}$ sec	$H_{max}$ ft	$H_{1/3,d}$ ft	$\bar{H}_d$ ft	$H_{min}$ ft	$H_{mo}$ ft
A0811, layout 3									
2	2.09	2.09	2.09	2.11	0.064	0.064	0.064	0.063	0.090
18	2.09	2.09	2.10	2.11	0.005	0.004	0.004	0.004	0.006

Figure 6 shows the incident wave conditions for the example case. This figure includes a surface elevation time series, frequency spectrum, and cumulative probability distribution (CPD) for the wave height. Time series, spectral, and CPD plots for all gages in each case in the regular wave series have been archived.

The incident wave pattern at gage 2 for all wave conditions in this test series is very linear and monochromatic. Agreement is excellent between target and measured wave periods. Wave height values are very closely grouped around the target value, indicating a very regular wave train. The time series plots are sinusoidal-shaped, without any evidence of nonlinear interactions (as would be indicated by a sawtooth wave shape, high frequency oscillations, or an overall low frequency beat pattern). The spectral plots also support this conclusion, with sharp single peaks at the peak frequency and no evidence of harmonic peaks. Also, the vertical alignment (like a step function) of the CPD plots indicates a very regular wave train.

Figure 7, similar to Figure 6, shows the transformed wave conditions inside the harbor for this example case. Again, time series, spectral, and CPD plots for all interior gage locations in this test series are archived. Some nonlinear effects of harbor transformation are observed in these plots. While wave periods showed little variation, wave heights did exhibit scatter. Figure 7 illustrates the emergence of sub- and higher harmonics along the back wall of the harbor. The long period beat effect, characteristic of wave grouping and sub-harmonics, is slightly evident in the time series plots. Also, higher harmonics manifest themselves in the small perturbations in the shape of the wave profile near the crests and troughs. The emergence of a subharmonic (frequency  $f$  approximately  $= 0.03 \text{ Hz}$ ) and the first two harmonics at  $f = 0.96$  and  $1.44 \text{ Hz}$  are barely evident in the spectral plots. The CPD plots are characterized by three vertical segments. The lower segment near  $H/H_{rms} = 0.6$  represents the higher frequency harmonic growth where  $H_{rms}$  equals the root-mean-square (RMS) wave height, in feet. The middle segment near  $H/H_{rms} = 0.7$  characterizes the primary wave, and the third segment near  $H/H_{rms} = 0.8$  represents the low-frequency subharmonic growth.

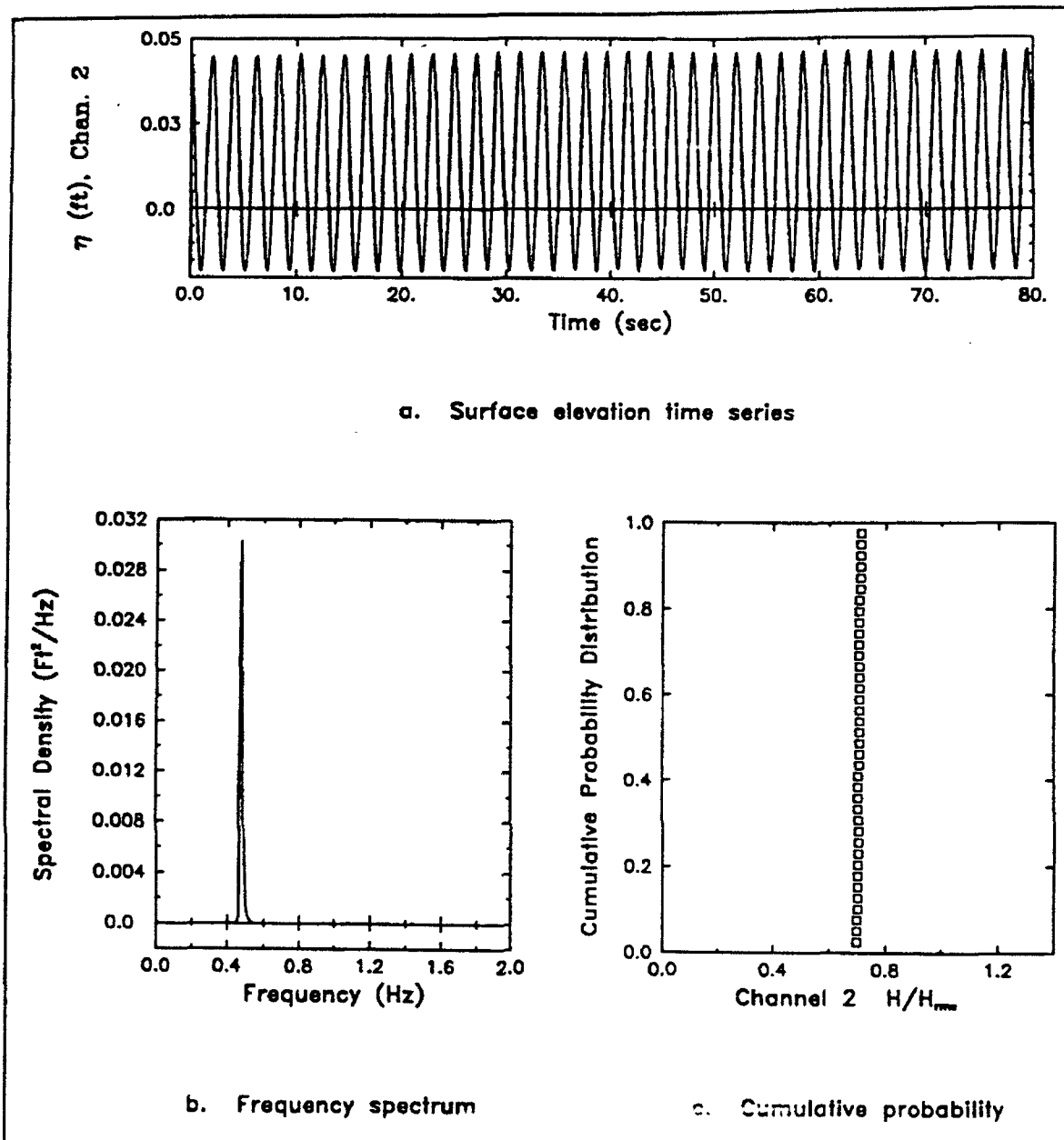


Figure 6. Incident gage 2 for regular wave case A0811, layout 3

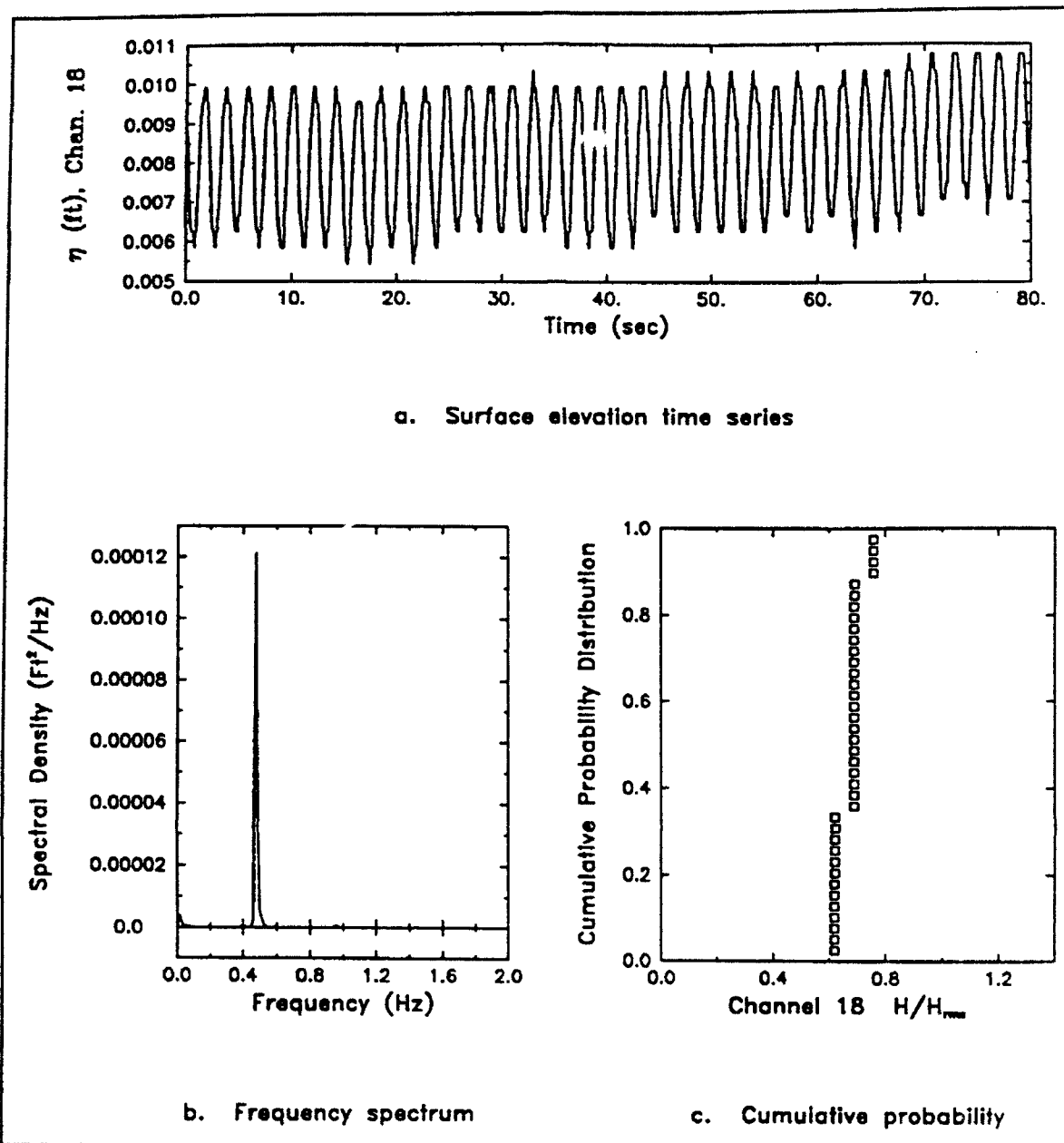


Figure 7. Harbor gage 18 for regular wave case A0811, layout 3

## Channel Entrance

The objective of the channel entrance series was to study wave transformation within the channel prior to contamination from reflected waves within the harbor. Two-hundred-and-forty combinations of wave and gage locations (i.e., 6 waves x 2 gage layouts x 20 gages per layout) were collected in each of the reflective and low-reflective phases. Case G08, corresponding to the low-reflective case A08 for the regular wave series, was selected as an example. Entrance channel gage 18 in layout 1 is on the channel center line, approximately 50 ft from the north wall of the harbor. Time for wave G08 to travel from gage 18 to the back wall and return is approximately 20 sec. Therefore, only 9 to 10 waves were analyzed to prevent contamination of the wave record with reflected energy.

The analysis for the channel entrance series is similar to that for the regular wave series. Table 10 lists the measured zero-downcrossing wave periods and heights for the incident and interior gages. A complete listing for all gages is given in Appendix D. Incident conditions measured at gage 2 are shown in Figure 8. Similarly, Figure 9 shows entrance channel conditions from gage 18. A complete set of plots for all gages in each of the channel entrance series is available in the archived data.

Gage No.	$\bar{T}_d$ sec	$T_{H_{1/3,d}}$ sec	$T_{H_{1/2,d}}$ sec	$T_{p,c}$ sec	$H_{max}$ ft	$H_{1/3,d}$ ft	$\bar{H}_d$ ft	$H_{min}$ ft	$H_{mo}$ ft
<b>G0803, layout 1</b>									
2	2.09	2.09	2.08	1.82	0.069	0.067	0.065	0.063	0.092
18	2.09	2.10	2.08	1.82	0.028	0.028	0.027	0.026	0.038

Incident wave periods and heights are similar to case A08 in the regular wave series. Observed variation is due to the shorter duration of the measured records. The time series plots are sinusoidal-shaped, without any evidence of nonlinear interactions. The spectral plots are wider than case A08, because the frequency resolution is not as good for the shorter duration records. No harmonic peaks are observed, either low or high frequency. The CPD is nearly vertical, another indication of a regular wave train.

Wave period remains invariant along the length of the entrance channel. Wave height first increases at the entrance and decreases toward the harbor to 40 percent of its original value. The time series and spectral plots indicate that the second harmonic has formed at  $f = 0.96$  Hz. The

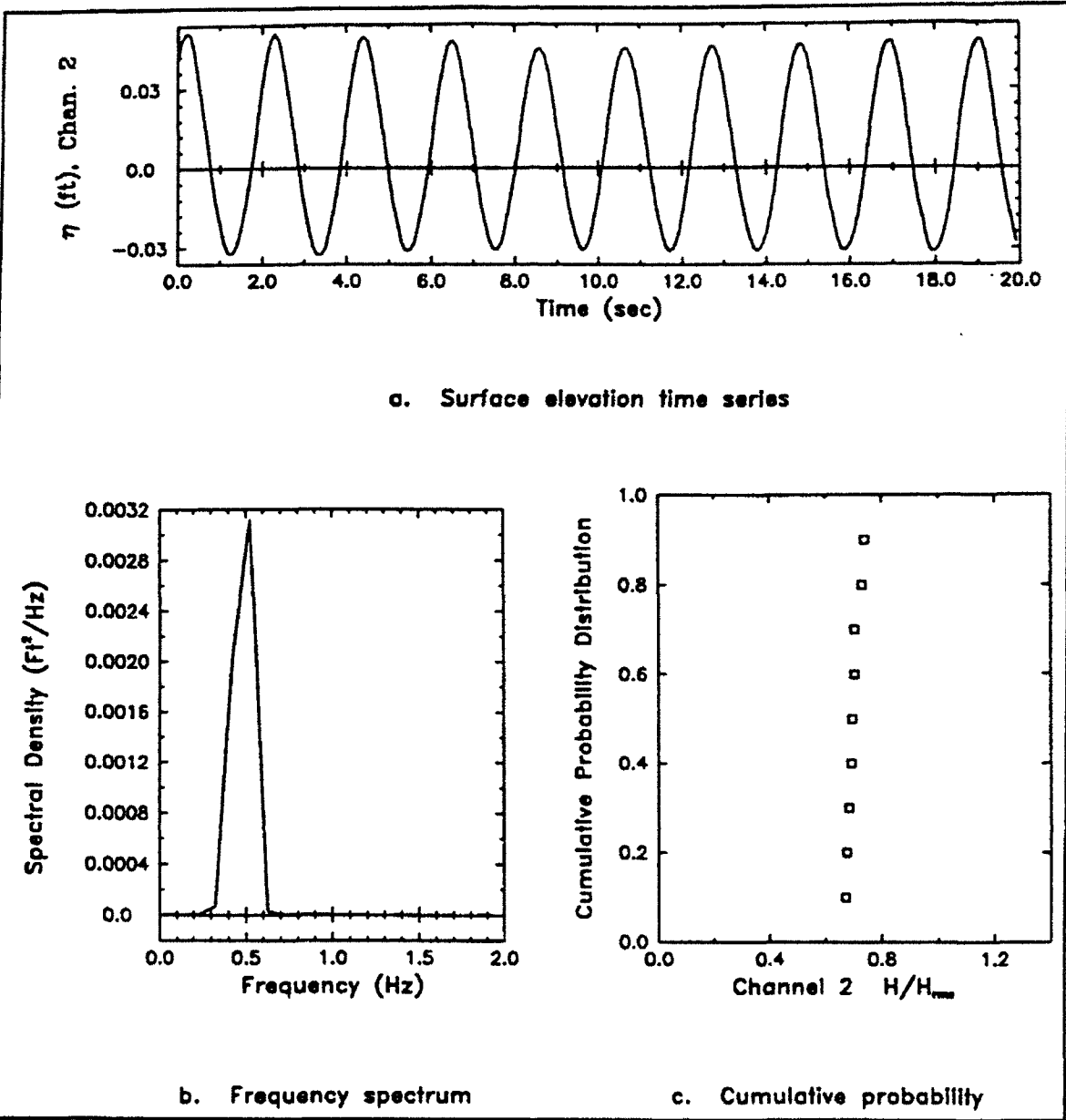


Figure 8. Incident gage 2 for channel entrance wave case G0803, layout 1

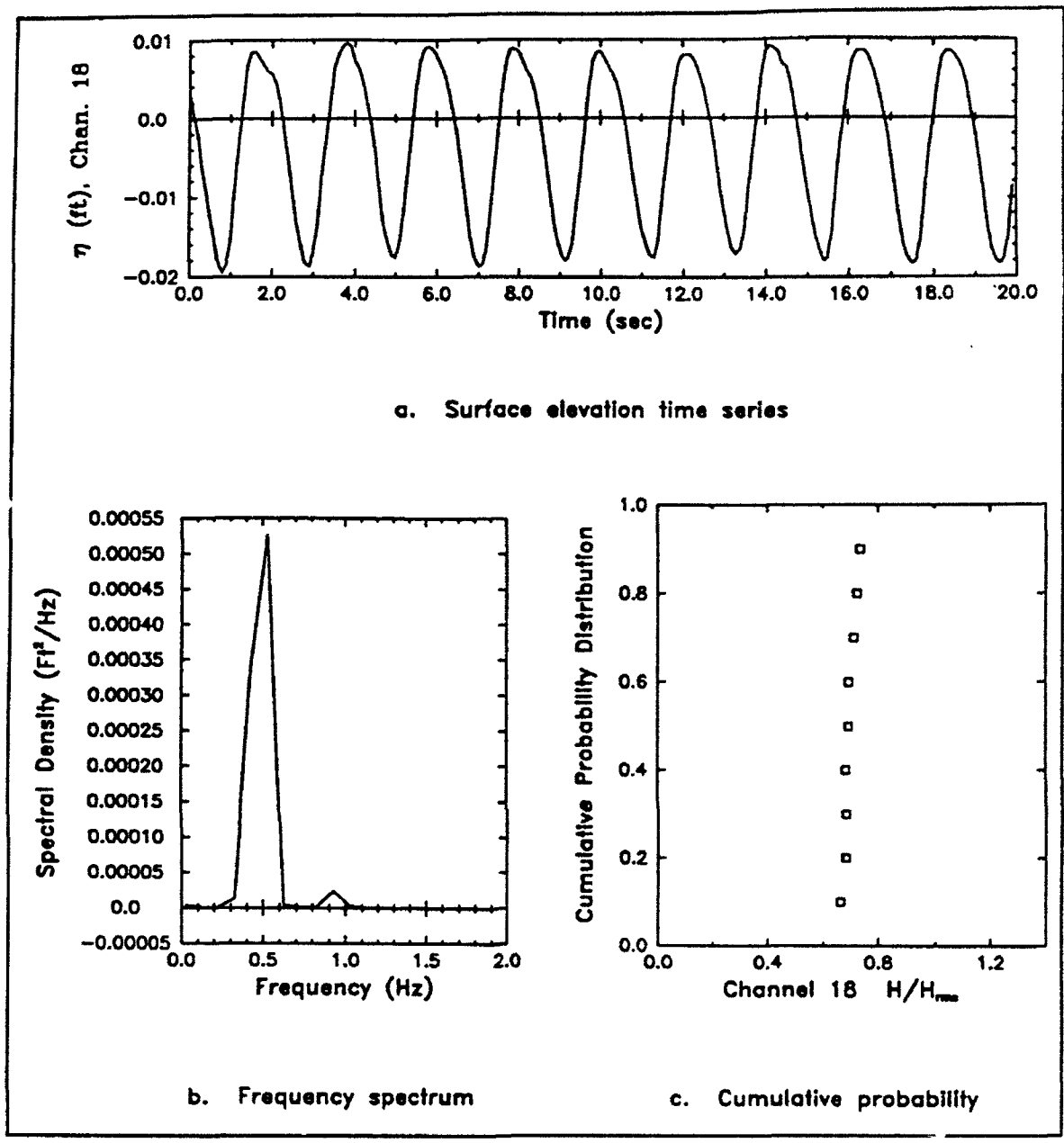


Figure 9. Harbor gage 18 for channel entrance wave case G0803, layout 1

CPD plot does not show any significant change from the incident plot, because of the shortage of points in the record.

## Harbor Resonance

Free long period waves, with wave periods corresponding to first and second modes along the longitudinal and transverse axes, were tested to see how accurately theoretical resonant modes were reproduced in the physical model. Eight hundred combinations of wave and gage location (i.e., 4 waves x 5 gage layouts x 20 gages per layout x 2 wall conditions) were collected.

Figure 10 illustrates the fundamental (first harmonic) and second mode shapes for a harbor with a closed basin. These wave profiles are typical of standing wave patterns due to perfect reflection from a vertical wall. The first mode has one node in the center of the basin and one antinode at each wall. The length of the basin in this direction corresponds to half a wavelength. The water surface appears to pivot about the nodal point in the middle of the basin. The displacement at the two antinodes is 180 deg out-of-phase with each other at any instant in

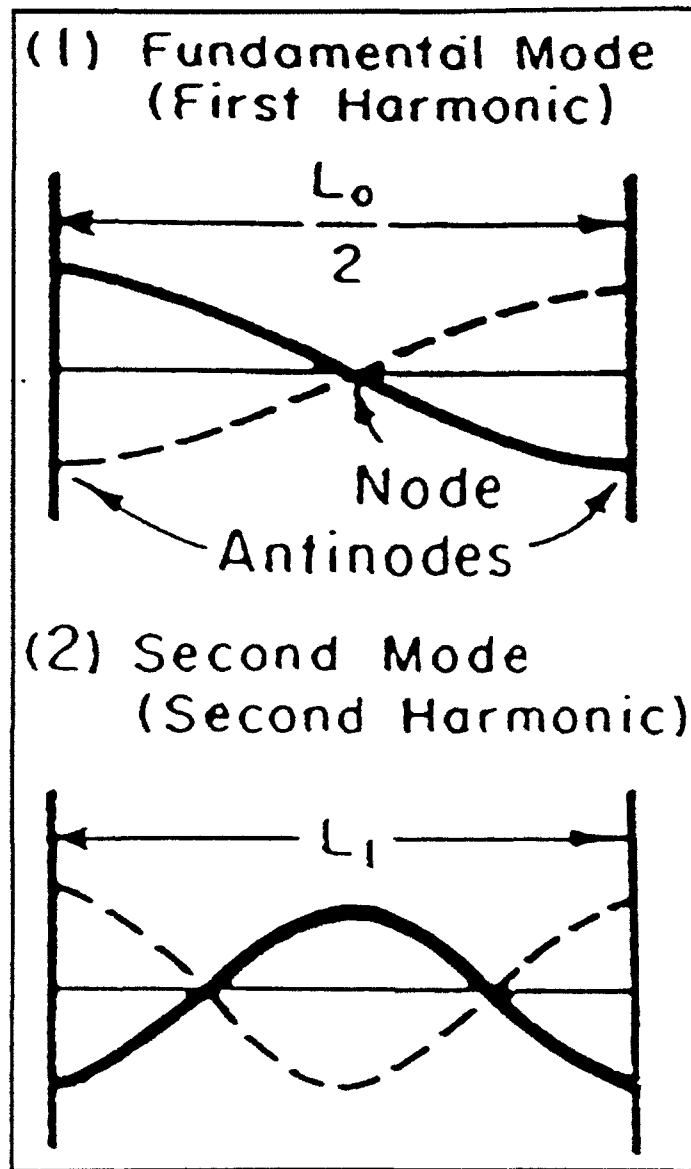


Figure 10. First and second mode shapes for an idealized harbor

time; a positive water level on one side of the nodal point is matched by an equivalent negative water level on the other side of the nodal point. The water surface at the antinodes goes from its highest to lowest values over half a wave period. There is no flow through the wall, so the horizontal velocity is zero at the antinode locations. The horizontal flow is greatest at the nodal point, a fact that influences surge motions of moored ships.

The second mode has two nodes and three antinodes. The nodes are evenly spaced in the basin and the additional antinode is located in the center of the basin. The water surface displacement is in phase for the two antinodes at the walls and 180 deg out-of-phase for the center antinode. The two nodal points again pose the greatest problem for ship surge.

If the period of the forcing waves (i.e., long period or infragravity waves) corresponds with the period of one of these modes, the amplitude at the antinodes can theoretically grow with time. However, natural dissipation mechanisms, such as bottom friction and wall absorption, tend to prevent this from happening. The total infragravity wave height measured in a harbor is typically less than 1.5 ft, much smaller than the energy in the wind wave range. Since a harbor will have first and higher order modes for longitudinal, transverse, and diagonal directions, the excursion at the antinodes at any one mode will be much less than this value.

Case E24, with a wave period of 17.7 sec, was selected as an example. This case corresponds to the first longitudinal (i.e., fundamental or first harmonic in Figure 10) mode of the harbor. Results will be shown for gages 2, 3, and 11 in layout 5 for case E24 (Run 8). Gage 2 is the incident wave condition. Gages 3 and 11 are parallel to the longitudinal axis of the harbor, along the north wall. Gage 3 is closest to the center of the harbor and gage 11 is in the north corner of the harbor, on the projection of the center line of the entrance channel. Table 11 lists measured wave periods and heights for these three gages. A complete listing of measured wave periods and heights for each gage and layout in this series is given in Appendix D. Harbor conditions measured at gages 2, 3, and 11 are shown in Figures 11, 12, and 13, respectively.

<b>Table 11 Measured Wave Periods and Heights for Harbor Resonance Series</b>									
<b>Gage No.</b>	$\bar{T}_d$ sec	$T_{H1/3,d}$ sec	$T_{H1/2,d}$ sec	$T_{p,c}$ sec	$H_{max}$ ft	$H_{1/3,d}$ ft	$\bar{H}_d$ ft	$H_{min}$ ft	$H_{m0}$ ft
<b>E2408, layout 5</b>									
2	17.69	17.73	17.67	17.65	0.066	0.065	0.064	0.061	0.090
3	17.70	17.65	17.72	17.65	0.162	0.161	0.159	0.141	0.221
11	17.68	17.71	17.86	17.65	0.211	0.210	0.207	0.196	0.290

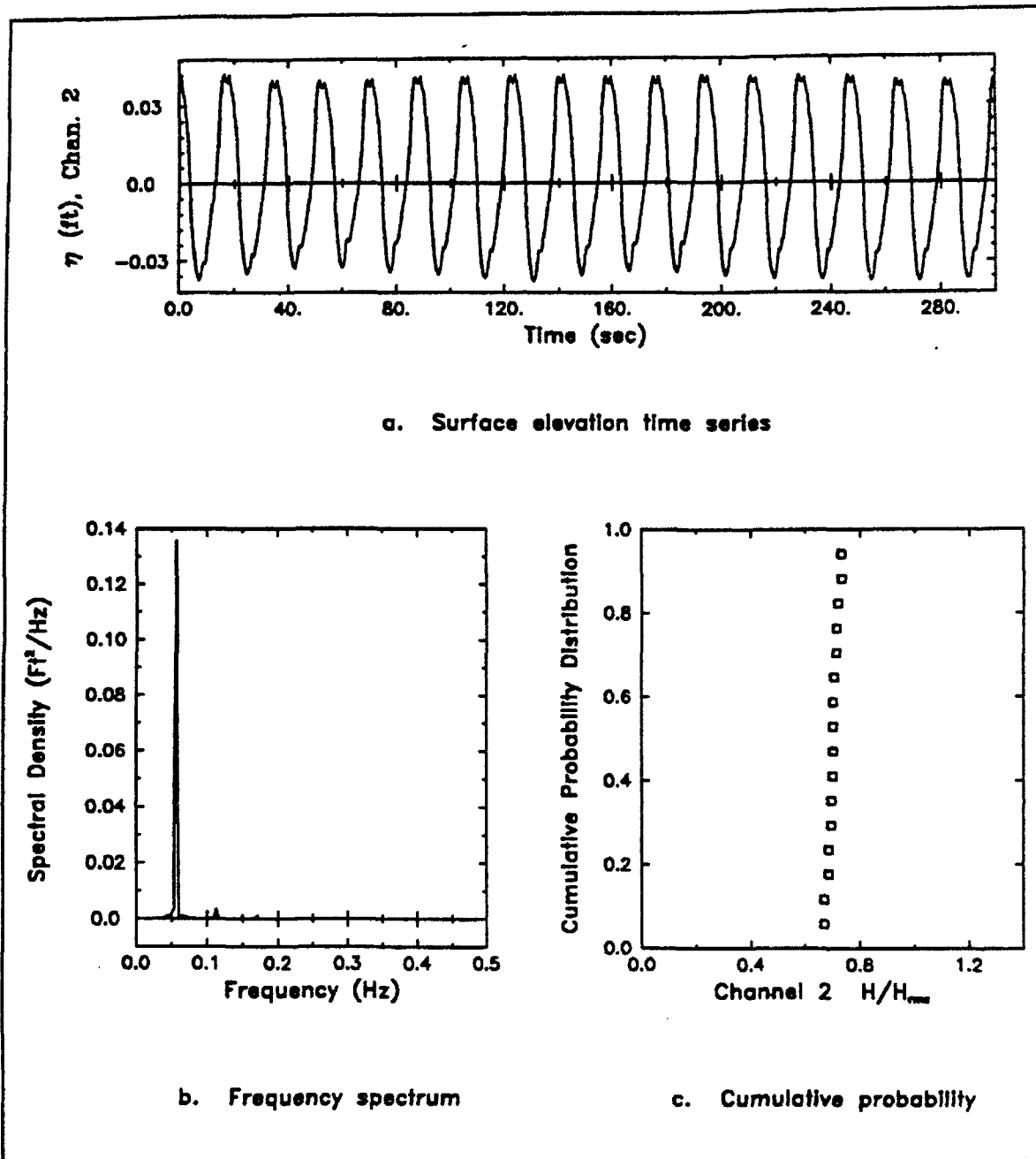


Figure 11. Incident gage 2 for harbor resonance wave case E2408, layout 5

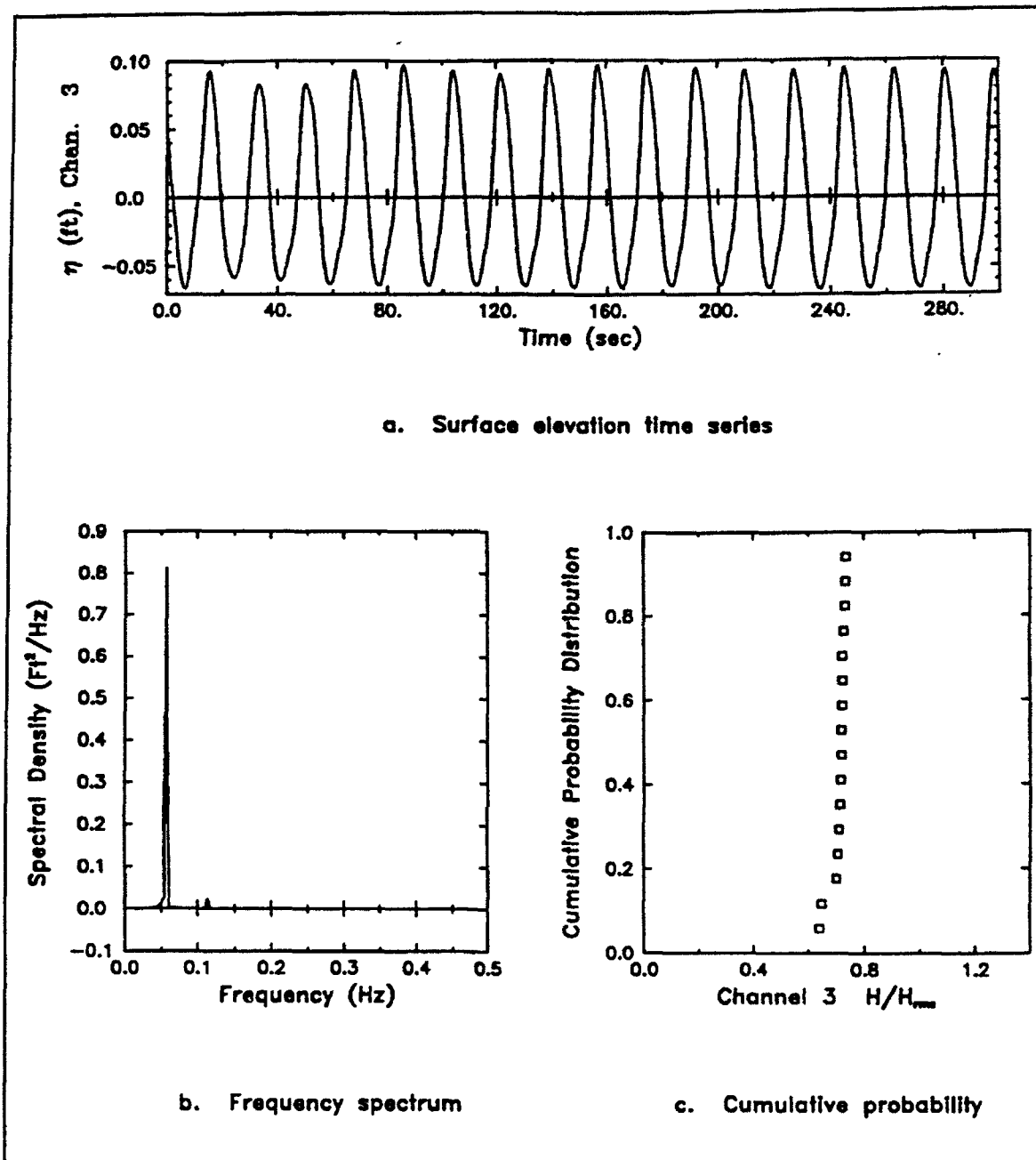


Figure 12. Harbor gage 3 for harbor resonance wave case E2408, layout 5

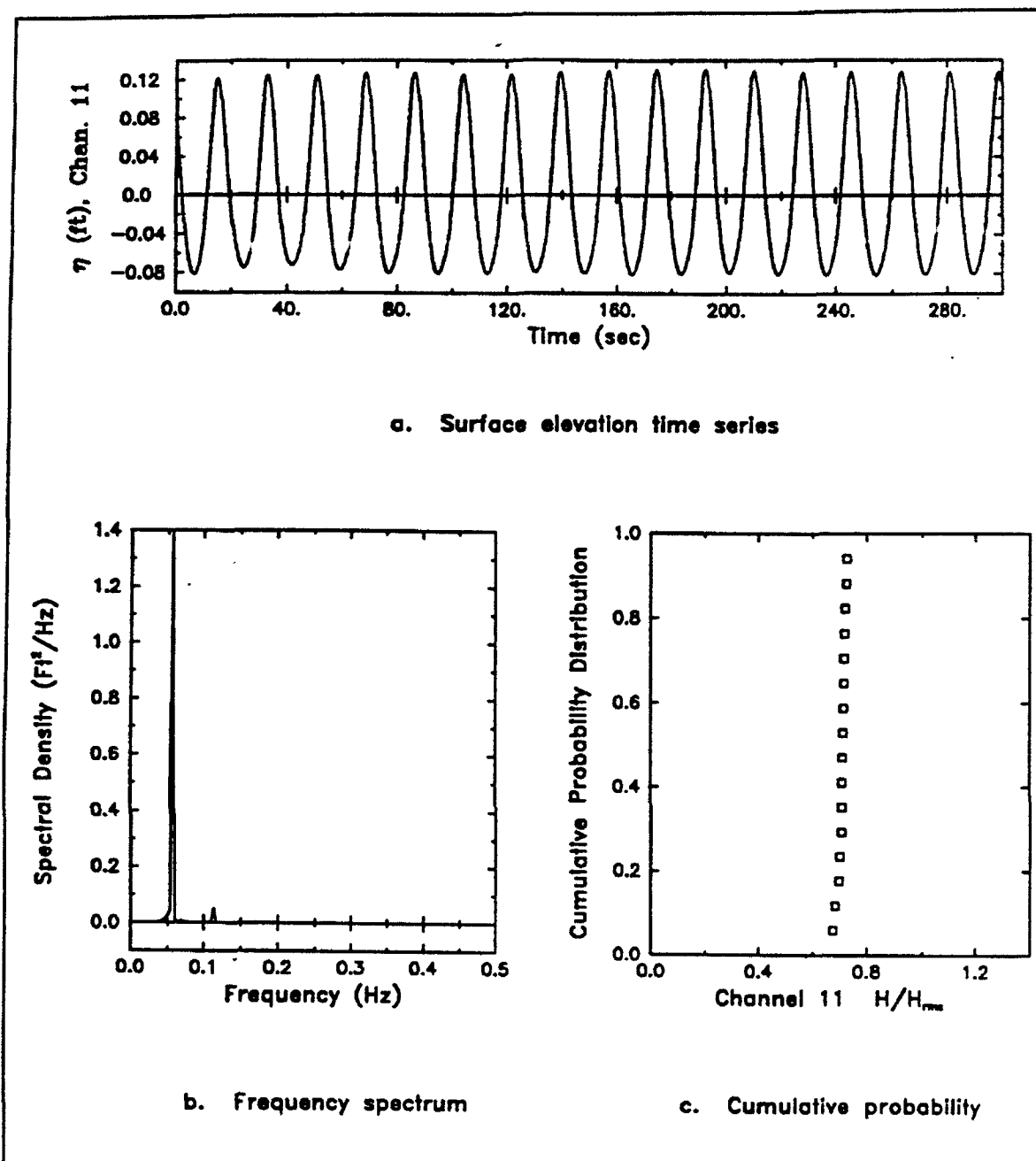


Figure 13. Harbor gage 11 for harbor resonance wave case E2408, layout 5

Figure 11 shows the incident conditions for this long wave. Because the wave period is so long, the wave is not as uniform as the previous waves discussed in the regular wave and channel entrance series. This effect from the second and third harmonics is illustrated by (a) the rough edges on the crests and troughs of the time series, (b) the harmonic peaks in the frequency spectra, and (c) the deviation from vertical in the cumulative probability curve. These higher harmonic effects are probably due to reflections from the beach and the back (north) wall of the harbor because the wave period of this wave is so large.

The resonant wave period remains constant at approximately 17.7 sec. Wave height increases by over 300 percent from incident conditions near the antinode at gage 11 due to harbor resonance. Wave height decreases linearly from gage 11 to gage 3, a pattern representative of the mode shape for the first mode (Figure 10), but is still almost 2.5 times greater than the incident value. The higher harmonic at  $f = 0.12 \text{ Hz}$  in the spectral plot is due to the reflected waves within the basin.

Preliminary analysis of the three mode shapes for first transverse (1w) and second longitudinal (2l) and transverse (2w) indicates reasonably good agreement. The mode shape for the second modes looks like the second harmonic in Figure 10, with the alignment being parallel to the longitudinal or transverse directions of the harbor. The 2l mode appears to be closer to the 1w mode because the resonant periods were fairly close (i.e.,  $T_{1w} = 9.9 \text{ sec}$  and  $T_{2l} = 9.0 \text{ sec}$ ).

## Wave Group

The objective of the wave group series was to explore the nonlinear transfer of energy from incident wave frequencies to the group frequency as waves travel into the harbor. A highly grouped incident wave was created by combining a pair of regular waves with nearly the same frequencies. Monochromatic wave frequencies, representative of wind wave frequencies, were chosen so that the difference between them matched an expected resonant frequency of the harbor.

Physical model data were collected for 300 combinations of wave and gage locations (i.e., 3 waves x 5 gage layouts x 20 gages per layout) for both reflective and low-reflective phases. Gage 3 in layout 2 for case F25 (Run 12) was selected as an example. This gage is in the west corner of the harbor.

The analysis for the wave group series is similar to that for the regular wave series. Table 12 lists the measured zero-downcrossing wave periods and heights for the incident and interior gages. A complete listing for all gages is given in Appendix D. Incident conditions measured at gage 2 are shown in Figure 14. Similarly, Figure 15 shows interior harbor conditions

<b>Table 12 Measured Wave Periods and Heights for Wave Group Series</b>									
<b>Gage No.</b>	$\bar{T}_d$ sec	$T_{H1/2,d}$ sec	$T_{H1/2,d}$ sec	$T_{p,c}$ sec	$H_{max}$ ft	$H_{1/3,d}$ ft	$\bar{H}_d$ ft	$H_{min}$ ft	$H_{m0}$ ft
<b>F2512, layout 2</b>									
2	1.08	1.06	1.06	1.11	0.131	0.124	0.095	0.007	0.132
3	1.59	1.49	5.66	10.00	0.006	0.006	0.005	0.002	0.009

from gage 3. A complete set of plots for all gages in each of the wave group test series is available in the archived data.

Test results matched expectations for highly grouped waves. The incident wave frequencies at 1.00 ( $1/T_{p,c} = 1/1.00$ ) and 0.90 ( $1/T_{p,c} = 1/1.11$ ) Hz have nearly vanished and an energetic long wave has emerged at 0.10 Hz ( $T_{p,c} = 10.0$ ), although the energy level is greatly reduced relative to the energy at  $T_{p,c}$  for the incident waves. The long wave frequency closely matches the difference between incident regular wave frequencies. The shift of energy from incident frequencies to the difference frequency is very clearly shown.

## Irregular Waves

Irregular waves were created to study the effects of frequency and directional spreading and nonlinear wave-wave interactions on the harbor response. Three irregular wave series were created to study broad ("B" cases) and narrow ("C" cases) frequency spreading for unidirectional waves and broad frequency and directional spreading ("D" cases) in the directional spectra series. Six hundred combinations of wave and gage location (i.e., 6 waves x 5 gage layouts x 20 gages per layout) were collected for both reflective and low-reflective phases. The example cases B02, C02, and D02 for the three series correspond to the A08 case for the regular wave series. The same interior harbor location (i.e., gage 18 in layout 3) was selected.

The analysis for the irregular wave series is similar to that for the regular wave series. Table 13 lists the measured zero-downcrossing wave periods and heights for the incident and interior gages. A complete listing for all gages is given in Appendix D. Incident conditions measured at gage 2 are shown in Figures 16 to 18 for the three examples. Similarly, Figures 19 to 21 show interior harbor conditions from gage 18. A complete set of plots for all gages in each of the irregular wave series is available in the archived data.

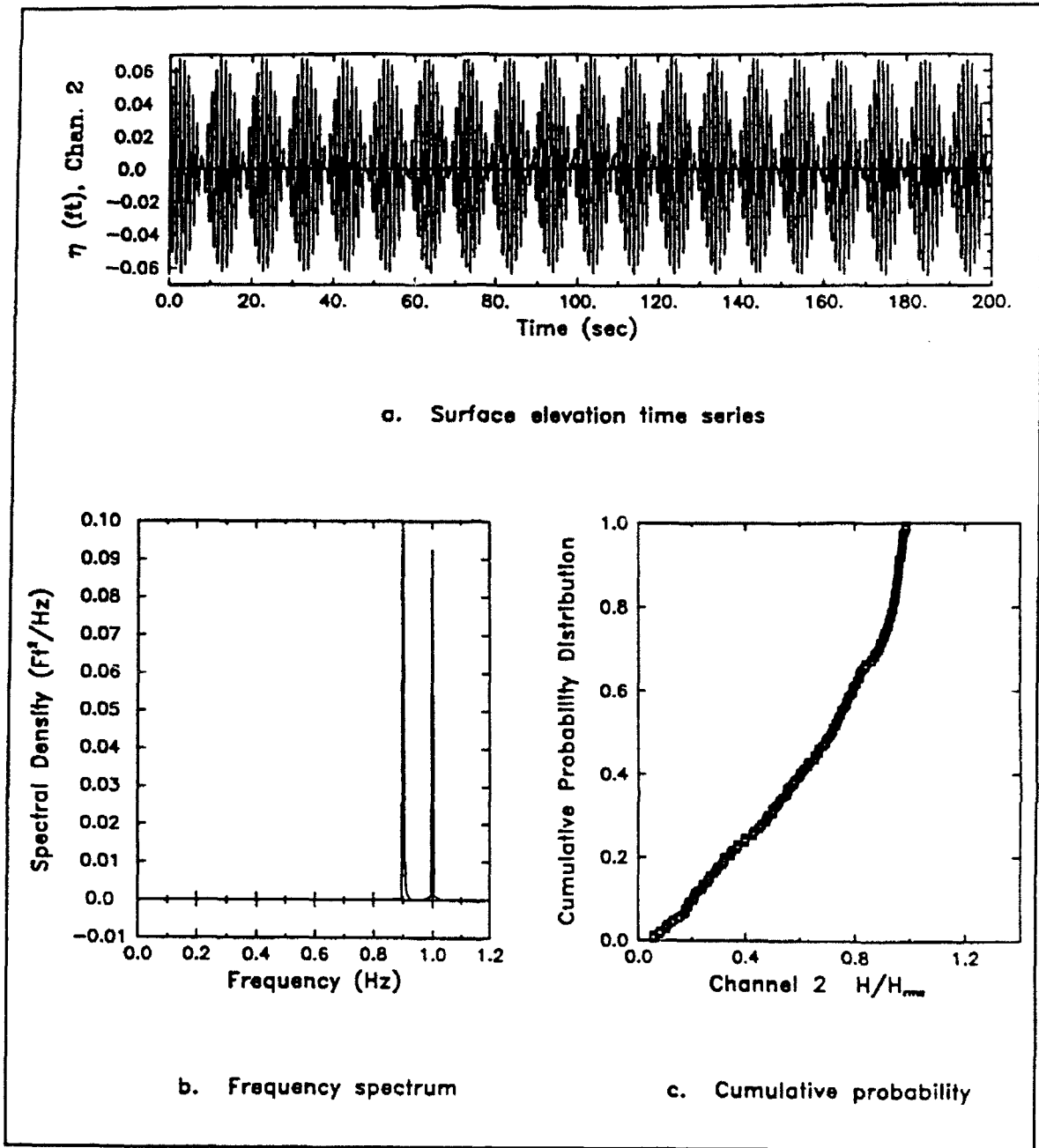


Figure 14. Incident gage 2 for wave group wave case F2512, layout 2

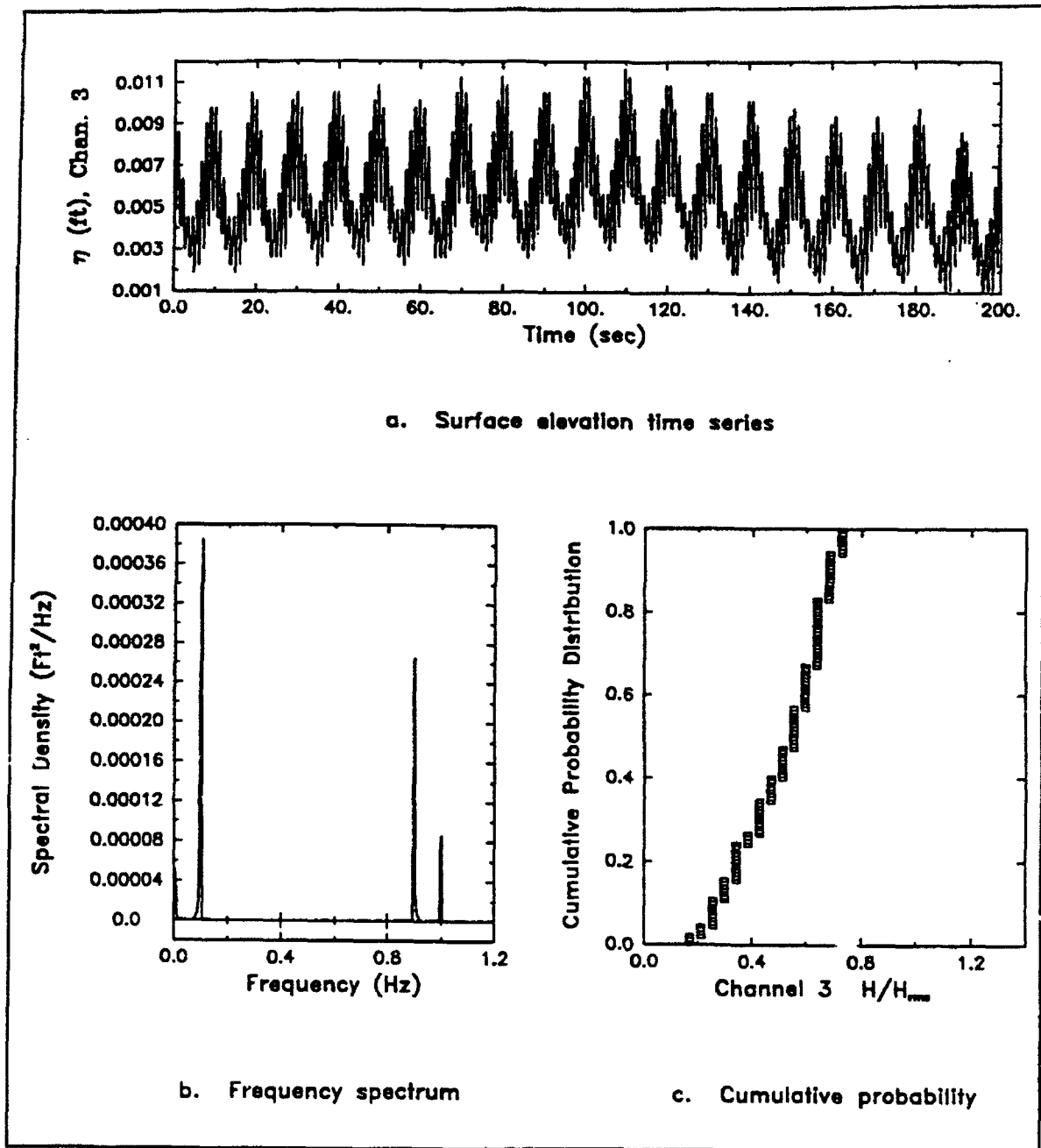


Figure 15. Harbor gage 3 for wave group wave case F2512, layout 2

<b>Table 13 Measured Wave Periods and Heights for Irregular Wave Series</b>									
<b>Gage No.</b>	$\bar{T}_d$ sec	$T_{H1/3,d}$ sec	$T_{H1/2,d}$ sec	$T_{p,c}$ sec	$H_{max}$ ft	$H_{1/3,d}$ ft	$\bar{H}_d$ ft	$H_{min}$ ft	$H_{mo}$ ft
<b>B0210 (Broad Frequency Spread, Unidirectional), layout 3</b>									
2	1.17	1.40	1.51	2.15	0.144	0.082	0.048	0.003	0.088
18	2.03	2.72	1.85	73.33	0.009	0.006	0.004	0.001	0.007
<b>C0210 (Narrow Frequency Spread, Unidirectional), layout 3</b>									
2	1.29	1.59	1.66	2.13	0.137	0.083	0.048	0.002	0.088
18	2.09	2.68	2.48	20.95	0.011	0.006	0.004	0.001	0.007
<b>D0210 (Broad Frequency and Directional Spread, Directional), layout 3</b>									
2	1.62	1.77	2.09	2.13	0.161	0.092	0.053	0.005	0.096
18	2.03	2.05	1.88	1.92	0.009	0.006	0.004	0.001	0.007

The irregular waves were calibrated in the calibration phase using a linear array of wave gages. Target spectral parameters were matched over the spatial extent of this array. The measured wave periods and heights for the incident gage 2 match the target values within confidence intervals for individual gages. Spectral wave periods match target periods better than zero-downcrossing periods. The frequency spreading in case C02 is narrower than the other two cases. The narrower spectrum is slightly more grouped than the wider spectrum with more zero-crossings. The spectral peak for the case C02 is more peaked than the wider case B02. The CPD plots are characterized by an even distribution of wave heights over all frequencies, typical of the irregular nature of spectral waves.

The interior harbor gage 18 records are characterized by a pronounced beat pattern, similar to the wave group series. Wave heights are significantly reduced relative to the incident values, with a large portion of the energy contained in the low frequencies. The spectral plots indicate that the same nonlinear transformation of energy occurs at multiple difference frequencies as occurred in the wave group series for the single monochromatic pairs. The spectral shape at the wind-wave frequencies is similar to the incident shape. Directional spreading in case D02 appears to reduce the amount of low-frequency energy relative to the unidirectional case B02. The CPD plots have the characteristic shape of a beat pattern.

Additional analysis with the irregular series data is warranted. Both linear and nonlinear processes are responsible for the observed changes in waves as they travel into the harbor interior. If linear mechanisms are responsible for most of the energy transfer, frequency response functions of gain, phase, and coherence can be used to evaluate the wave transformation.

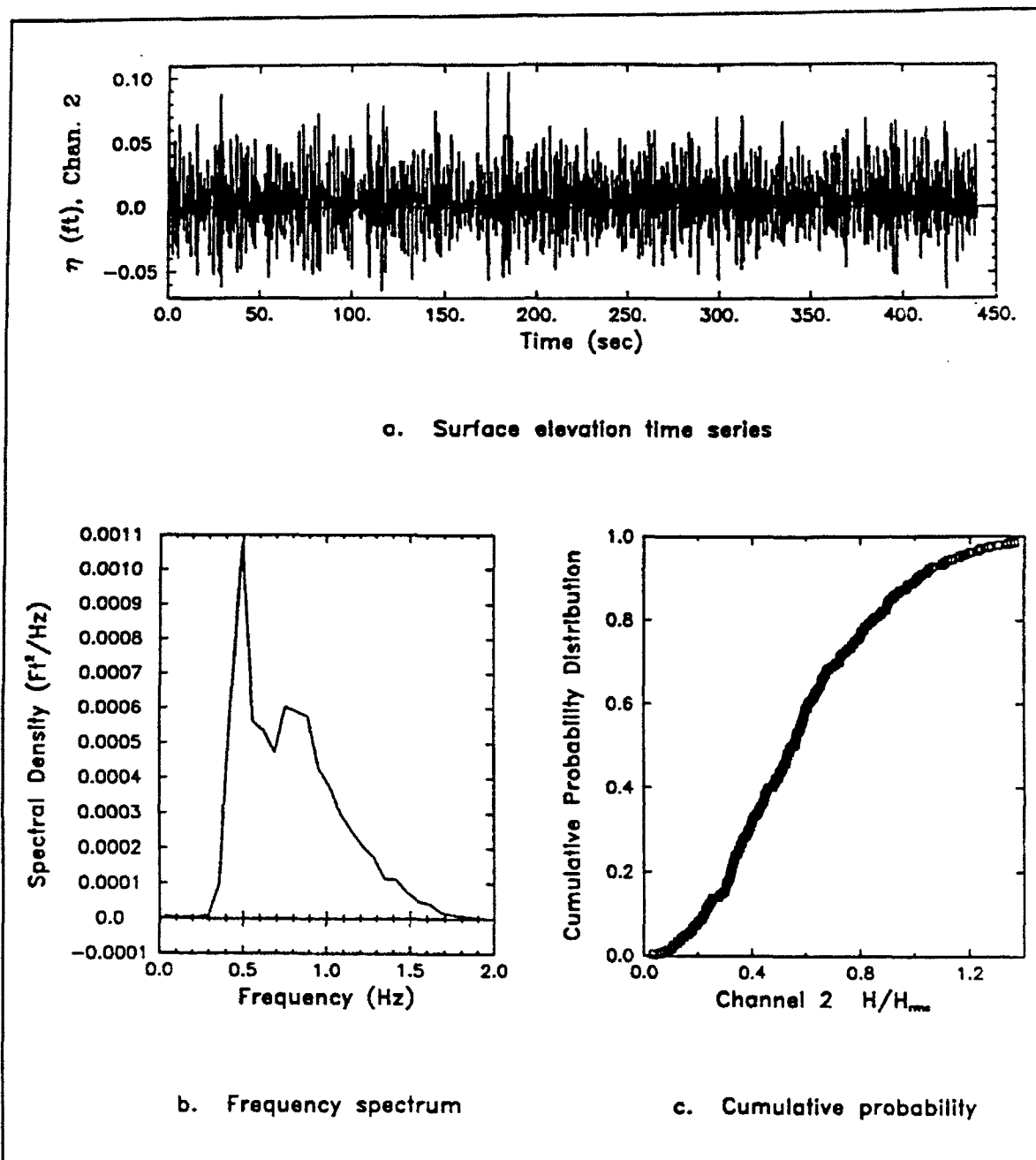


Figure 16. Incident gage 2 for irregular wave case B0210, layout 3

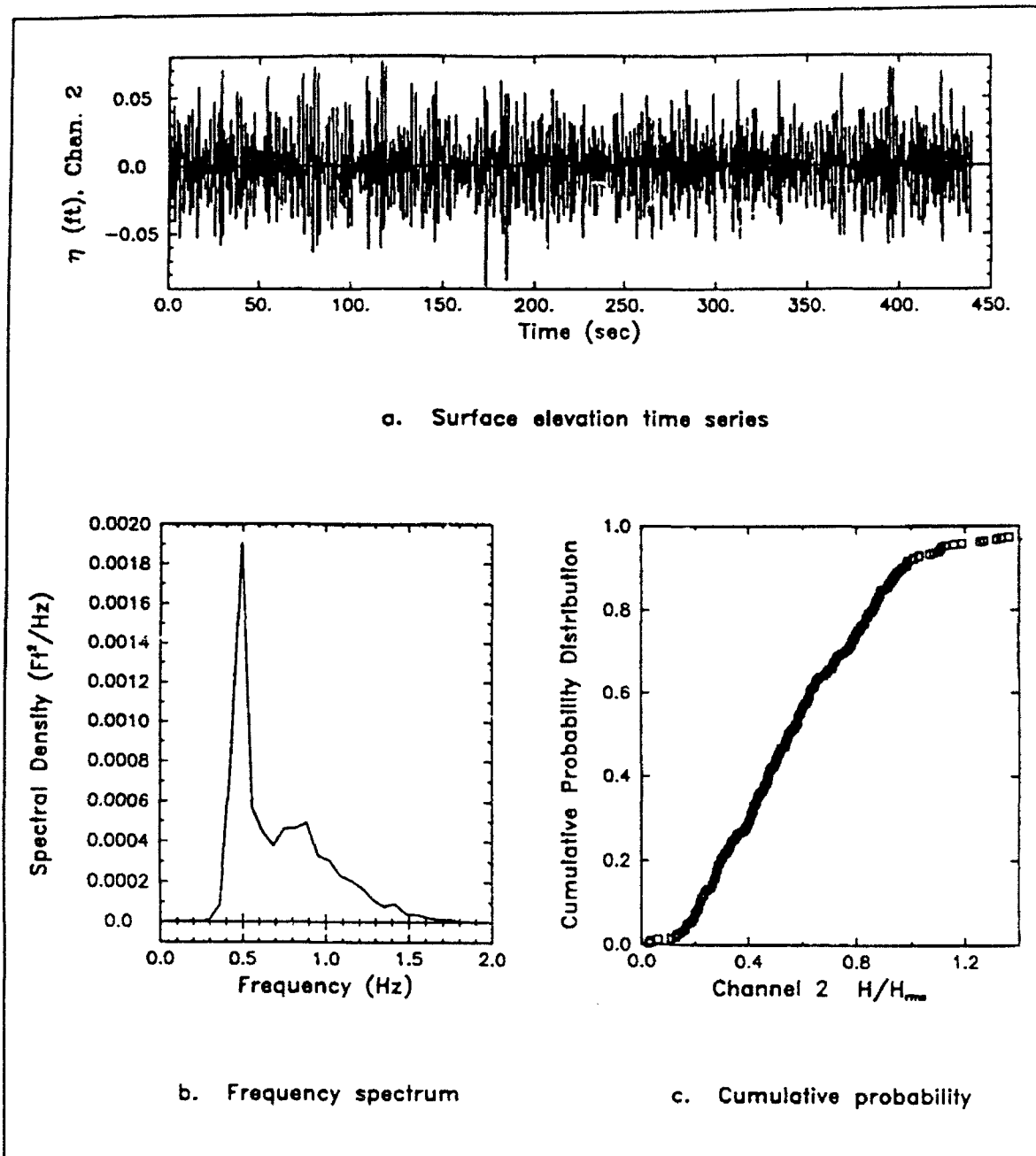


Figure 17. Incident gage 2 for irregular wave case C0210, layout 3

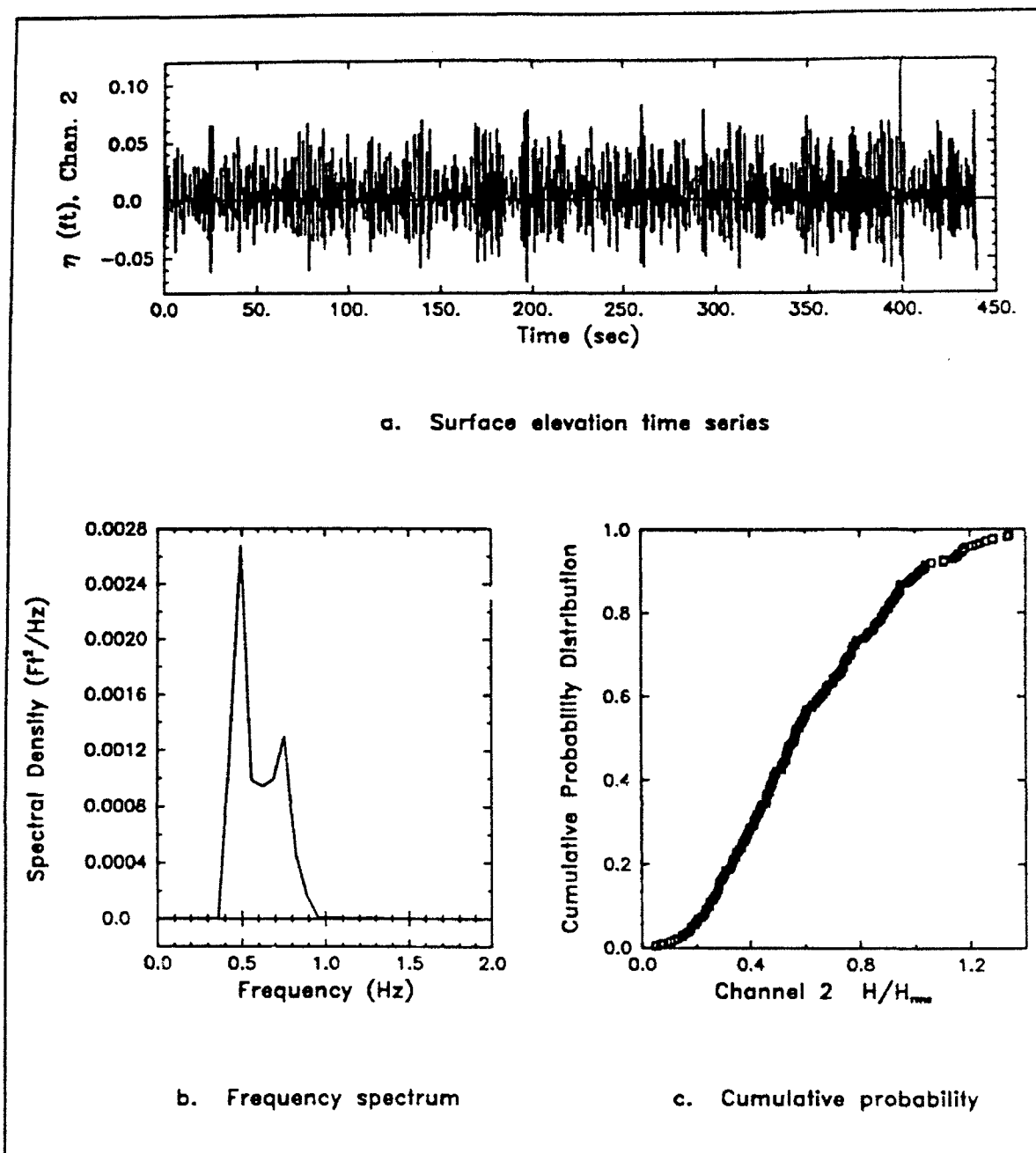


Figure 18. Incident gage 2 for irregular wave case D0210, layout 3

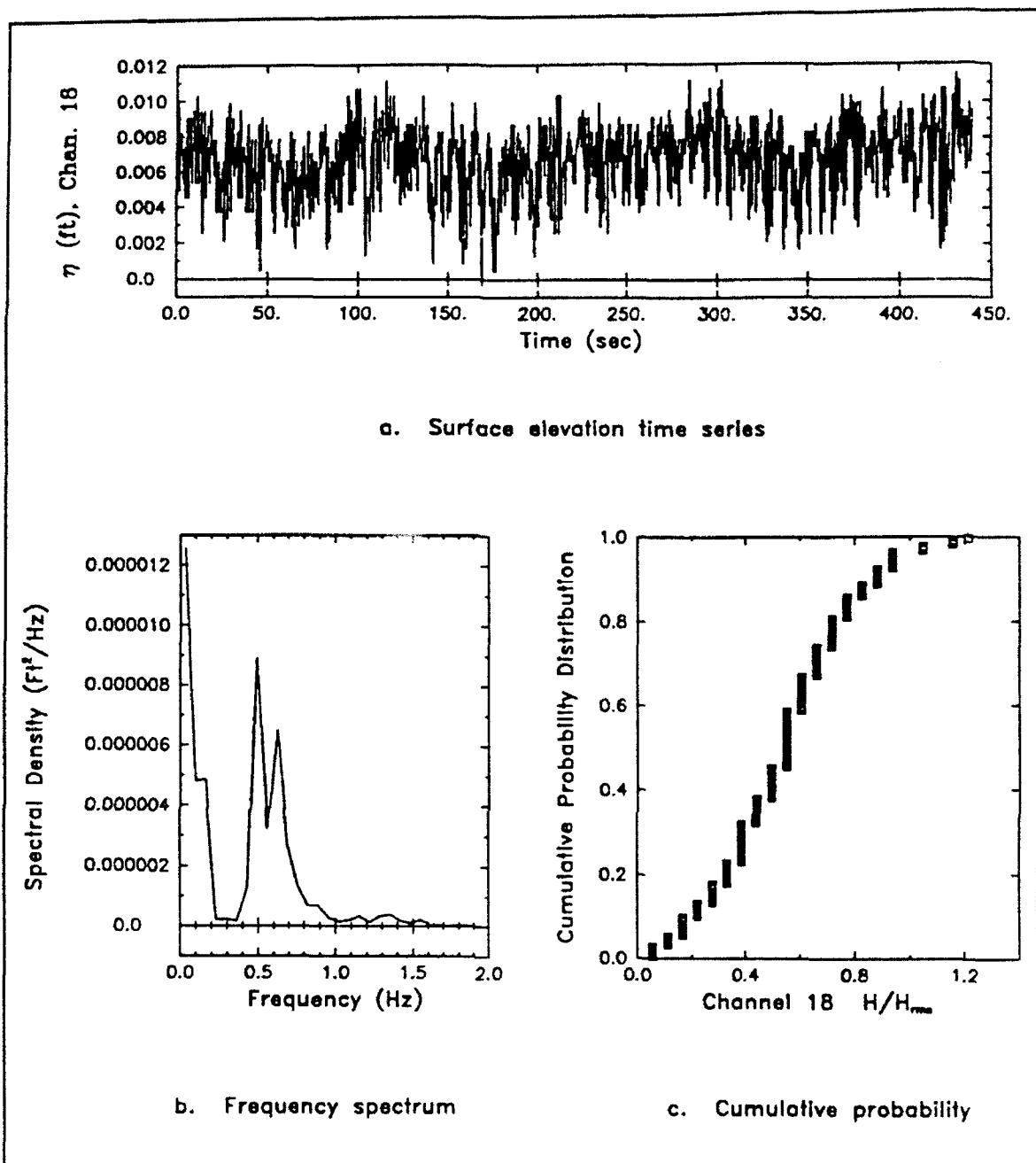


Figure 19. Harbor gage 18 for irregular wave case B0210, layout 3

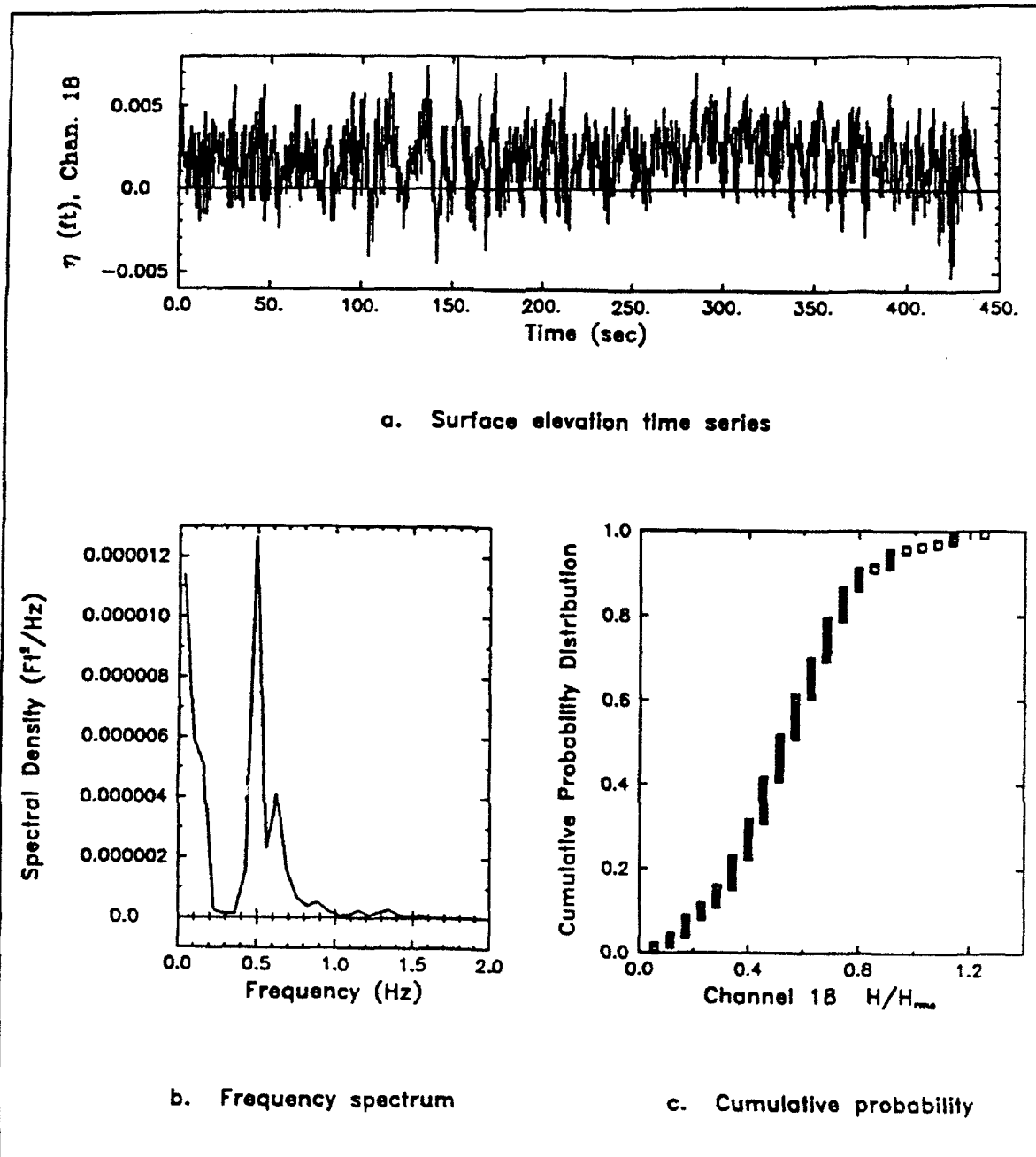


Figure 20. Harbor gage 18 for irregular wave case C0210, layout 3

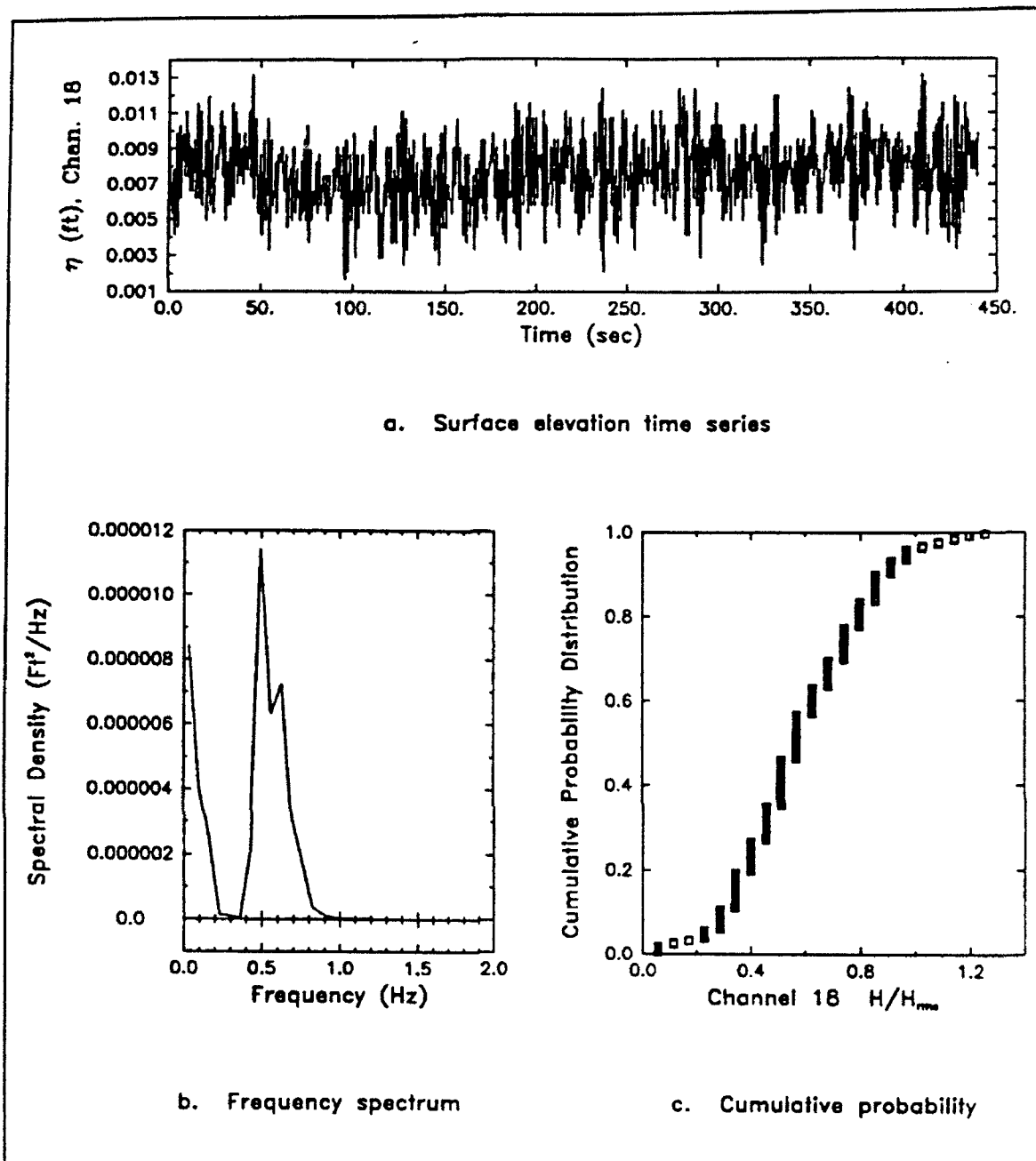


Figure 21. Harbor gage 18 for irregular wave case D0210, layout 3

Linear theory does not predict the growth of harmonics and subharmonics, which can lead to harbor resonance. One method used to detect these nonlinear wave-wave interaction mechanisms is bispectral analysis. Future work could investigate the cross-bicoherence between the incident gage 2 and interior harbor gages to quantify the extent of this nonlinear interaction.

## Wave-Current

The objective of the wave-current phase was to study the effect of an ebb current on wave parameters outside the entrance channel. Four-hundred-and-eighty combinations of wave and gage locations (i.e., 12 waves x 1 gage layout x 20 gages per layout x 1 low-reflective wall condition x 2 wave-current conditions) were collected with wave gages. The twelve waves included the six waves in the regular and irregular wave series. The two wave-current conditions were waves only and waves with current. Current only and wave-current data were collected with four current meters, but these data are not reported here.

Case A06, corresponding to case A06 for the regular wave series, was selected as an example. This wave is aligned parallel to the entrance channel with an overall wave direction of  $\theta = -22.5$  deg. Gage 18 is on the channel center line, closest to the channel, so it should show the largest effect of the 0.5-knot ebb current. Gage 3 is approximately 2.5 channel widths from the mouth of the channel.

The analysis for the wave-current phase is similar to that for the regular wave series. Table 14 lists the measured zero-downcrossing wave periods and heights for wave only (run 14) and wave with current (run 15) at gages 3 and 18. A complete listing for all gages is given in Appendix D. Gage 3 wave conditions for wave only and wave plus current are shown in Figures 22 and 23, respectively. Similarly, Figures 24 and 25 show the

<b>Table 14</b>									
<b>Measured Wave Periods and Heights for Wave-Current Phase</b>									
Gage No.	$\bar{T}_d$ sec	$T_{H1/3,d}$ sec	$T_{H1/2,d}$ sec	$T_{p,c}$ sec	$H_{max}$ ft	$H_{1/3,d}$ ft	$\bar{H}_d$ ft	$H_{min}$ ft	$H_{m0}$ ft
<b>A0614, wave only</b>									
3	2.09	2.09	2.09	2.11	0.084	0.084	0.083	0.083	0.116
18	2.09	2.09	2.09	2.11	0.070	0.070	0.069	0.069	0.103
<b>A0615, wave-current</b>									
3	2.09	2.09	2.09	2.11	0.097	0.095	0.093	0.090	0.133
18	2.09	2.09	2.10	2.11	0.108	0.107	0.105	0.102	0.146

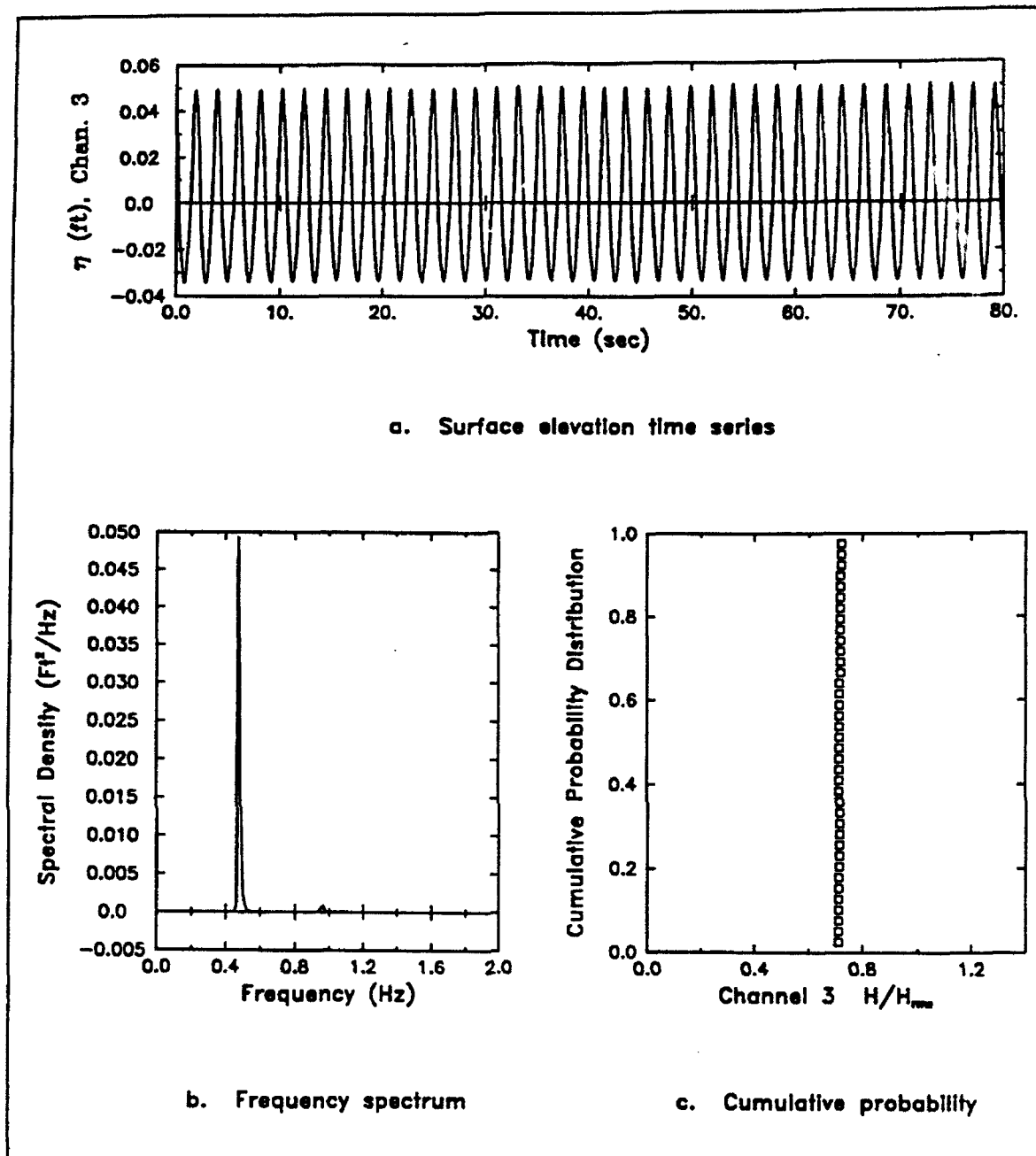


Figure 22. Channel gage 3 for wave case A0614, layout 1

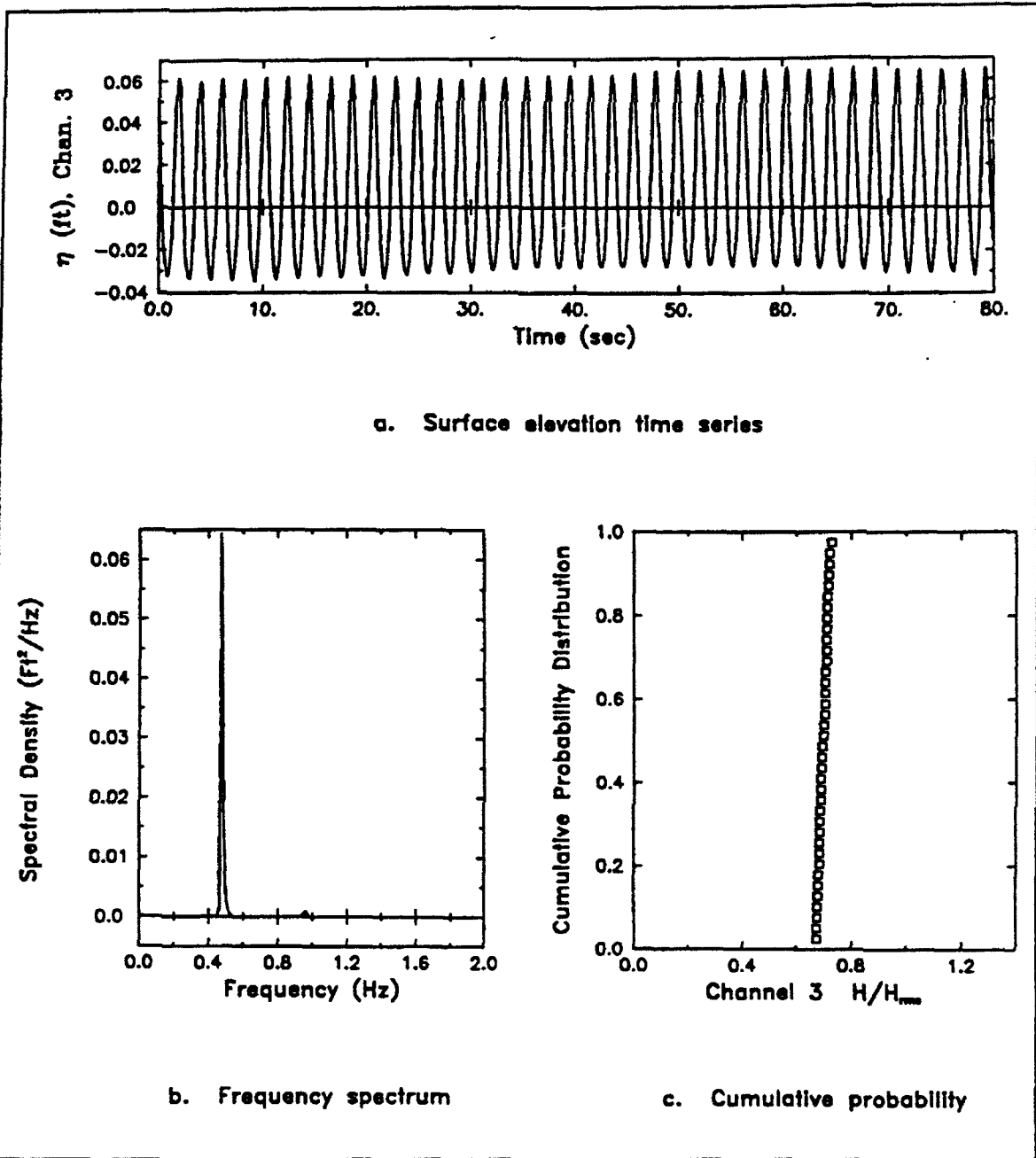


Figure 23. Channel gage 3 for wave-current case A0615, layout 1

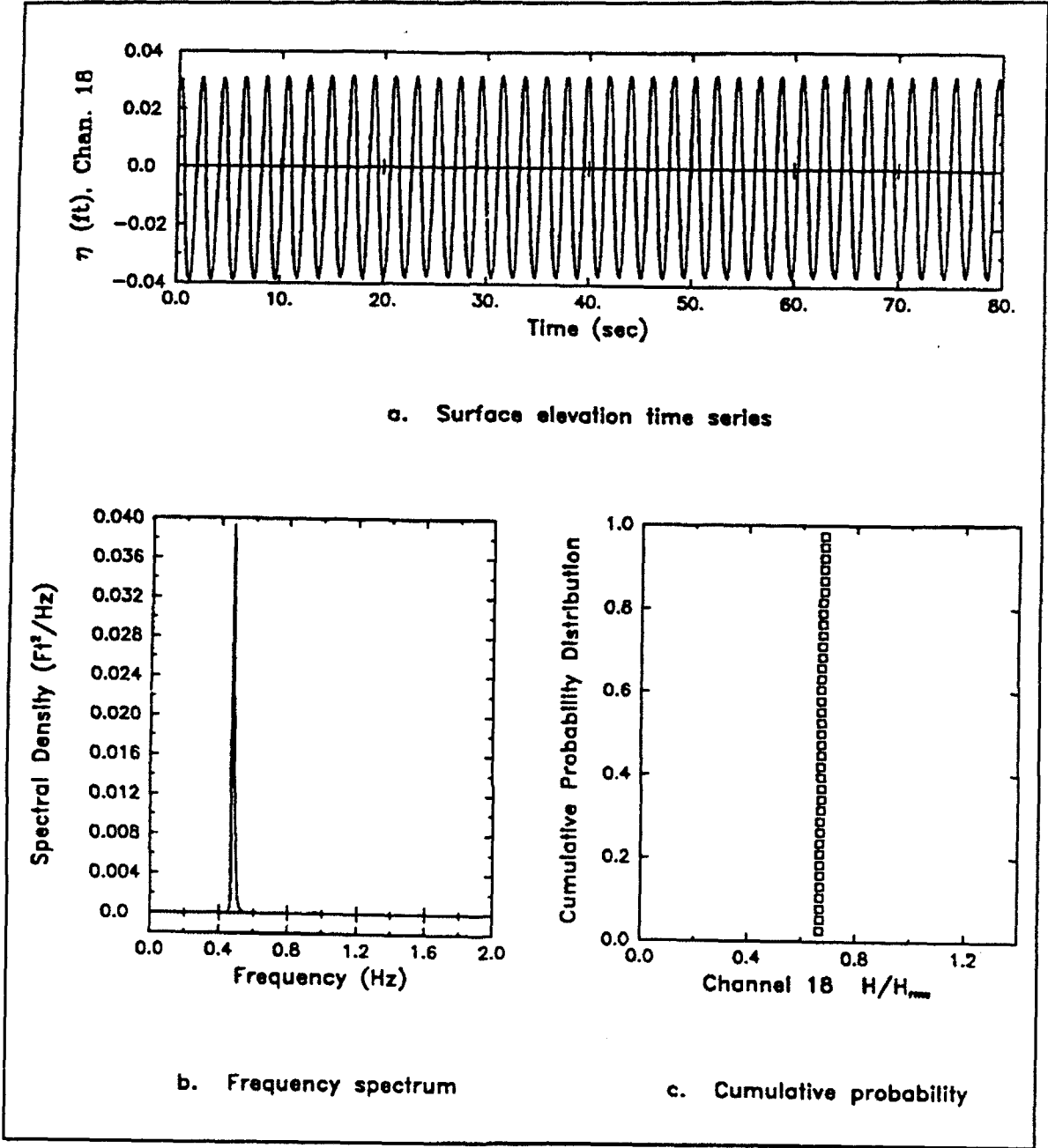


Figure 24. Channel gage 18 for wave case A0614, layout 1

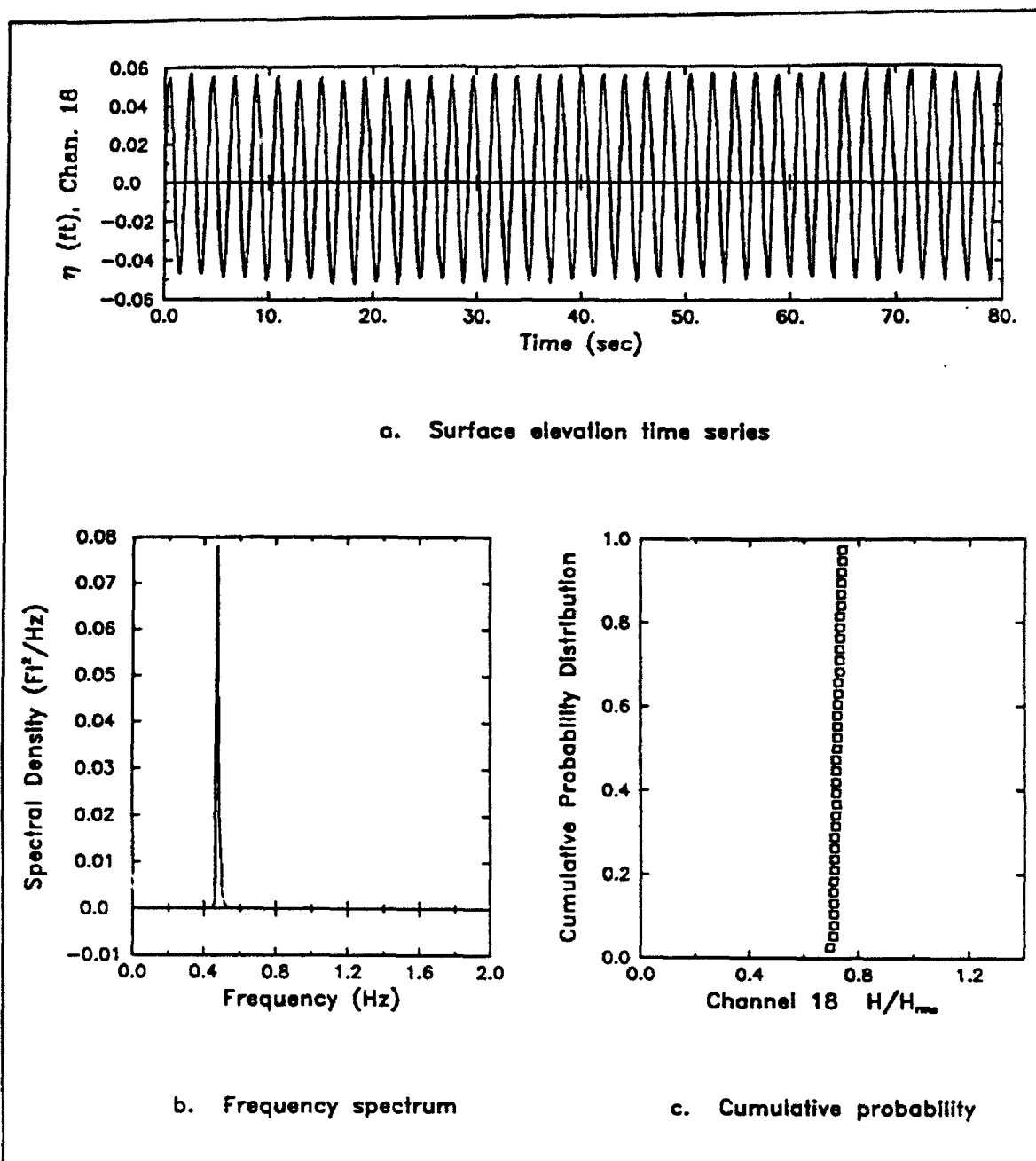


Figure 25. Channel gage 18 for wave-current case A0615, layout 1

effect of the current on wave patterns for gage 18. A complete set of plots for all gages in each of the wave-current phases is available in the archived data.

The presence of an ebb current does not affect the wave period, it remains unchanged at both gages 3 and 18. The wave height, however, is affected by the ebb current. The strength of the ebb current diminishes as it flows seaward, reducing its effect on wave height. At gage 18 closest to the mouth of the channel, wave height increases by 50 percent (i.e.,  $0.105/0.069$ ) due to the presence of the ebb current. The time series and spectral plots both increase and the CPD plot is no longer vertical, indicative of the steepening experienced by the wave due to the opposing current. Furthest offshore at gage 3 (approximately 2.5 channel widths offshore), the effect of the current was not as pronounced, wave height was only 12 percent (i.e.,  $0.093/0.083$ ) greater due to the current.

The effects of refraction, shoaling, and wave breaking on wave transformation are seen by comparing gages 3 and 18 for both wave only and wave-plus-current environments. Wave height decreases 17 percent (i.e.,  $0.069/0.083$ ) without the current, but increases 13 percent due to the current. Thus, the effect of the current must have been even greater to offset the loss in wave height due to refraction and breaking.

Additional analysis with this data is planned to predict the effect of ebb currents on wave conditions seaward of an entrance channel. The effect of *ebb currents flowing through an idealized inlet on regular waves* was investigated in the Cornell study (Briggs and Green 1992). Comparisons with this data set are planned.

## 4 Summary and Conclusions

---

A three-dimensional, 1:45-scale physical model of an idealized, rectangular flat-bottom harbor, entrance channel, and nearshore bathymetry was constructed in CERC's directional spectral wave basin. Extensive laboratory measurements were collected during a wide variety of regular and irregular waves and ebb currents to study the effects that frequency and directional spreading, harbor resonance, wave grouping, and wave-current interaction have on harbor response. Typical prototype wave periods were 8 and 14 sec (1.19- and 2.09-sec model). A prototype wave height of 3.75 ft (1-in. model) was selected for all tests to prevent overtopping and breaking and minimize nonlinear interactions. Waves had principal wave directions of 0 and  $\pm 22.5$  deg ( $-22.5$  deg is parallel to the entrance channel). Tidal ebb currents of 0.5 knot (0.88 fps prototype, 0.13 fps model) were created to study the wave-current interaction in the nearshore region outside the entrance channel. Boundary conditions in the harbor and channel included fully reflecting vertical walls and low-reflecting, 1:1.3 stone slopes. Twenty capacitance wave gages and four electromagnetic current meters in nine different gage configurations were used.

Data analyses consisted of time series plots, zero-downcrossing, and frequency spectral analysis. Measured zero-downcrossing wave periods  $T_d$ ,  $T_{H1/3,d}$ , and  $T_{H1/2,d}$  were calculated. Zero-downcrossing wave heights included  $H_{max}$ ,  $H_{min}$ ,  $H_{1/3,d}$ , and  $\bar{H}_d$  to characterize the distribution of wave heights. For the spectral analysis, the wave gage data were zero-measured, tapered by a 10-percent cosine bell window, and Fourier transformed to the frequency domain. Calculated results included peak wave period  $T_{p,c}$  and zero-moment wave height  $H_{m0}$ .

Predicted and measured reflection coefficients were calculated to accurately represent boundary conditions for use in numerical models. For the 1:6 beach slopes opposite the DSWG, measured reflection coefficients from the physical model and predicted reflection coefficients from Ahrens's (1987) work with rubble-mound reef breakwaters were calculated. For the 1:1.3 stone slopes lining the entrance channel and the harbor, only predicted values were provided.

The measured reflection coefficients exceeded predicted values except for the last three cases in the harbor resonance series. Goda's analysis assumes that incident and reflected waves travel parallel to the orientation of the two gages. Waves at an angle will probably produce erroneous results, the magnitude of which is not known. Therefore, engineering judgment should be used in selecting values for use in numerical models. Additional investigation and comparison of reflection coefficients with the HARBD numerical model should be conducted.

The incident wave pattern for the regular wave cases was very linear and sinusoidal, as evidenced by the time series and spectral plots. Agreement between target and measured wave periods and heights was excellent. Interior harbor gages indicated some nonlinear effects of harbor transformation in the form of long-period beat effects (subharmonics) and higher harmonics. While measured wave periods showed little variation, wave heights exhibited scatter due to these nonlinear effects.

The objective of the channel entrance series was to quantify wave transformation within the channel prior to contamination of the incident wave field by reflected energy. Wave period remained invariant along the length of the entrance channel. Wave height increased near the entrance and then decreased to 40 percent of its original value toward the harbor.

Free long-period waves, with wave periods corresponding to first and second modes along the longitudinal and transverse axes, were tested to see how accurately theoretical resonant modes were reproduced in the physical model. Response of the harbor to forcing from a wave corresponding to the first longitudinal mode (1l) agreed with predictions. Wave period remained constant at approximately 17.7 sec. Wave height at the antinodes (i.e., walls) increased by over 300 percent from incident conditions and decreased toward the node in the center of the harbor, a pattern representative of the mode shape for the first mode. Preliminary analysis of the three mode shapes for first transverse (1w) and second longitudinal (2l) and transverse (2w) indicated reasonably good agreement. The mode shape for the 2l mode appears to be closer to the 1w mode because the resonant periods were fairly close (i.e.,  $T_{1w} = 9.9$  sec and  $T_{2l} = 9.0$  sec).

Nonlinear transfer of energy from incident wind wave frequencies to wave group frequencies as waves travel into harbors can produce damaging long period harbor oscillations. Highly grouped incident waves were created by combining a pair of monochromatic waves with nearly the same frequency, both representative of wind wave frequencies. Test results matched expectations in that energy was transferred from incident wave frequencies to the long wave frequency. These data are expected to be very useful for other investigations of harbor seiching and resonance due to wave groups. For example, the Barbers Point Harbor, Oahu, Hawaii, study benefitted from the insight gained in this study.

Irregular waves were created to study the effects of frequency and directional spreading and nonlinear wave-wave interactions on harbor response. Three irregular wave series were created to study broad and narrow frequency spreading for unidirectional waves and broad frequency and directional spreading in the directional spectra series. Interior harbor gages were characterized by a pronounced beat pattern, similar to the wave group series. Wave heights were significantly reduced relative to the incident values, with a large portion of the energy contained in the low frequencies. Spectral plots indicate that the same nonlinear transformation of energy occurs at multiple difference frequencies as occurred in the wave group series for single monochromatic pairs. The spectral shape at the wind-wave frequencies is similar to the incident shape. Directional spreading appears to reduce the amount of low-frequency energy relative to cases without spreading.

The objective of the wave-current phase was to study the effect of an ebb current on wave parameters seaward of the entrance channel. In the vicinity of tidal inlets and river mouths, currents can significantly modify wave amplitude, form, and direction. For the case of an ebb current and waves parallel to the entrance channel, wave period remained invariant. Wave height was increased up to 50 percent in the presence of ebb currents. As the strength of the ebb current diminishes flowing seaward, its effect on wave height is reduced. Several channel widths offshore, wave height was still 12 percent greater than it would have been without the current. Additional analysis and comparison with the Cornell data set is planned to predict the effect of ebb currents on wave conditions seaward of an entrance channel.

Both linear and nonlinear processes are responsible for the observed changes in waves as they travel into the harbor. If linear mechanisms are responsible for most of the energy transfer, frequency response functions of gain, phase, and coherence can be used to evaluate wave transformation. Linear theory does not predict growth of harmonics and subharmonics, which can lead to harbor resonance. One method used to detect these nonlinear wave-wave interaction mechanisms is bispectral analysis. Future work should investigate the cross-bicoherence between the incident gage and interior harbor gages to quantify this nonlinear interaction.

Preliminary comparisons of the low-reflective phase of the regular series data with the numerical model HARBD were made. Results from these comparisons showed the importance of specifying the proper reflection and bottom friction coefficients. Additional analysis and comparisons with HARBD should be made to fully utilize the data's potential.

This report has described the laboratory data collection effort. This data set is being used with other laboratory data to provide insight into the complicated wave transformation mechanisms that influence harbors. Design guidance on the effects of frequency and directional spreading, nonlinear energy transfer among wave components, and wave-current interaction is being presented in technical notes and technical papers for

eventual placement in appropriate Engineering Manuals sponsored by the Engineering Division, Directorate of Civil Works.

## References

---

- Ahrens, J.P. (1987). "Characteristics of Reef Breakwaters," Technical Report CERC-87-17, U.S. Army Engineer Waterways Experiment Station, Vicksburg, MS, 1-45.
- Borgman, L.E. (1990). "Irregular Ocean Waves: Kinematics and Forces," *Ocean Engineering Science*, Part A, B. LeMehaute and D. Hanes, eds., Wiley-Interscience, New York, 121-168.
- Bowers, E. C. (1977). "Harbor Resonance Due to Set-down Beneath Wave Groups," *J. Fluid Mech.*, 7(1), 71-92.
- Briggs, M.J., Borgman, L.E., and Outlaw, D.G. (1987). "Generation and Analysis of Directional Spectral Waves in a Laboratory Basin," OTC 5416, Offshore Technology Conference, Houston, TX, 495-502.
- Briggs, M. J., and Smith, J. M. (1990). "The Effect of Wave Directionality on Nearshore Waves," International Conference on Coastal Engineering (ICCE), Delft, The Netherlands, July 2-6, 267-280.
- Briggs, M. J., and Boc, S. J. (1991). "Physical Model Testing of Barbers Point Harbor and Marina Complex," World Marina '91, Long Beach, CA, September 4-8, 391-401.
- Briggs, M. J., Lillycrop, L. S., and McGehee, D. D. (1992). "Comparison of Model and Field Results for Barbers Point Harbor," Coastal Engineering Practice '92, Long Beach, CA, March, 1992.
- Briggs, M. J. and Green, D. R. (1992). "Experimental Study of Monochromatic Wave-Ebb Current Interaction," Miscellaneous Paper CERC-92-9, U.S. Army Engineer Waterways Experiment Station, Vicksburg, MS.
- Chen, H. S. (1984). "Hybrid Element Modeling of Harbor Resonance," *Proceedings of the 4th International Conference on Applied Numerical Modeling*, 312-316.
- \_\_\_\_\_ (1986). "Effects of Bottom Friction and Boundary Absorption on Water Wave Scattering," *Applied Ocean Research*, 8(2), 99-104.

- Chen, H. S. and Mei, C. C. (1974). "Oscillations and Wave Forces in an Offshore Harbor," Report No. 190, Department of Civil Engineering, Massachusetts Institute of Technology, Cambridge, MA.
- Crawford, P.L., and Chen, H.S. (1988). "Comparison of Numerical and Physical Models of Wave Response in a Harbor," Miscellaneous Paper CERC-88-11, U.S. Army Engineer Waterways Experiment Station, Vicksburg, MS.
- Elgar, S., Guza, R. T., Freilich, M. H., and Briggs, M. J. (1992). "Laboratory Simulations of Directionally Spread Shoaling Waves," *ASCE WPCOE Journal*.
- Goda, Y., and Suzuki, Y. (1976). "Estimation of Incident and Reflected Waves in Random Wave Experiments," *Proceedings of the 16<sup>th</sup> International Conference on Coastal Engineering*, 828-845.
- IAHR Working Group on Wave Generation and Analysis. (1986). "List of Sea State Parameters," Supplement to Bulletin No. 52, January, 1-24.
- Kaihatu, J. M., and Berry, S. W. (1989). "Analysis and evaluation of laboratory wave-current data: harbor idealized tests (H.I.T.)," DF, Coastal Engineering Research Center, U.S. Army Engineer Waterways Experiment Station, Vicksburg, MS.
- Kirkegaard, J., and Nielsen, A. H. (1982). "Hydraulic Studies for Bintulu Deepwater Port," *Portech '82*.
- Lillicrop, L. S., Thompson, E. F., and Briggs, M. J. (1991). "Model Comparisons of Harbor Wave Response," *Coastal Zone '91*, Long Beach, CA, July 8-12, 894-903.
- Lillicrop L. S., and Briggs, M. J. 1992. "Design and Modification of Harbors: A Case Study," Coastal Engineering Technical Note (CETN), U.S. Army Engineer Waterways Experiment Station, Vicksburg, MS.
- Longuet-Higgins, M. S., and Stewart, R. W. (1962). "Radiation Stresses and Mass Transport in Gravity Waves with Applications to Surf-Beat," *J. Fluid Mech.*, 13, 481-504.
- Munk, W. H. (1949). "Surf beats," *EOS Trans. American Geophysical Union*, 30(6), 849-854.
- Noda, Edward K. and Associates, Inc. (1988). "Evaluation of Surge Forces for the Barbers Point Deep-draft Harbor," prepared for Nakamura and Tyau, Inc. and DOT, Harbors Division, State of Hawaii.
- Okihiro, M., and Seymour, R. J. (1992). "Barbers Point Harbor Resonance Study," Scripps Institution of Oceanography (unpublished manuscript).
- Okihiro, M., Guza, R. T., and Seymour, R. J. "Infragravity Bound Waves," *Journal of Geophysical Research*, in preparation.

Sand, S. E. (1982). "Wave Grouping Described by Bounded Long Waves," *Ocean Engng.*, 9(6), 567-580.

# Appendix A

## Notation

---

$a$	Wave amplitude
$B_e$	Resolution bandwidth, Hz
$C$	Wave celerity
$D(f,\theta)$	Wrapped normal directional spreading function
$f$	Frequency, Hz
$f_l$	Lower cutoff frequency, Hz
$f_p$	Spectral peak frequency, Hz
$f_u$	Upper cutoff frequency, Hz
$h$	Water depth, ft
$H$	Wave height, ft
$H_{\max}$	Maximum wave height, ft
$H_{\min}$	Minimum wave height measured, ft
$H_{m0}$	Zero-moment wave height, ft
$H_{\text{rms}}$	Root-mean-square (RMS) wave height, ft
$\bar{H}_d$	Average zero-downcrossing wave height
$H_{0.5}$	Average of the highest 1/2 of zero-downcrossing wave heights, ft
$H_{1/3,d}$	Zero downcrossing significant wave height, ft
$K_{r,m}$	Measured reflection coefficient from physical model, %

$K_{r,p}$	Predicted reflection coefficient from empirical data, %
$l$	$h \cot \theta$
$L$	Wavelength, ft
$L_p$	Wavelength at peak period, ft
NFIRST	First point analyzed
NTIME	Number of points in a record
$S_{TMA}(f)$	TMA frequency spectra
$T$	Wave period, sec
$\bar{T}_d$	Average wave period, sec
$T_{H1/2,d}$	Average of periods of the highest 1/2 of zero-downcrossing wave heights, sec
$T_{H1/3,d}$	Zero downcrossing significant period, sec
$T_{pc}$	Spectral peak period, sec
$T_r$	Time series duration, sec
$u_c$	
$u_{max}$	Maximum horizontal water particle velocity at the surface
$x_{13}$	Spacing between gages 1 and 3, 2 ft
$x_{18}$	Spacing between gages 1 and 8, 7 ft
$X$	Gage x-coordinate in the global system
$X'$	Gage x-coordinate in the physical model system
$X''$	Gage x-coordinate in the numerical model system
$y_1$	Distance along the y-axis between origins, 93.2 ft
$Y$	Gage y-coordinate in the global system
$Y'$	Gage y-coordinate in the physical model system
$Y''$	Gage y-coordinate in the numerical model system
$\gamma$	Spectral peakedness parameter

$\Delta f$	Basic frequency increment, Hz
$\Delta l$	Optimum gage spacings for reflection analysis
$\Delta t$	Time interval, sec
$\theta$	Component wave direction, deg Beach or breakwater slope, deg
$\vec{\theta}$	Overall mean wave direction for all frequencies, deg
$\sigma_m$	Mean spreading standard deviation
$\phi_y$	Offset phase angle controlling wave direction
$\nu$	Degrees of freedom

# **Appendix B**

## **Test Case Run Numbers**

---

**Appendix B-1  
Calibration Phase Run Numbers, Harbor Idealized Tests**

Test Case	Gage Layout			Wave Condition
	1	2	3	
A01	1,2	3,4,5	—	Regular
A02	1,2	3,4	—	Regular
A03	1	2,3	—	Regular
A04	1	2,3	—	Regular
A05	1	2,3	—	Regular
A06	1	2,3	—	Regular
A07	1	2,3	—	Regular
A08	1	2,3	—	Regular
B01	—	—	1,2	Irregular
B02	—	—	1,2	Irregular
C01	—	—	1,2	Irregular
C02	—	—	1,2	Irregular
D01	—	—	1,2	Irregular
D02	—	—	1,2	Irregular
E21	1	2	—	Harbor Res
E22	1	2	—	Harbor Res
E23	1	2	—	Harbor Res
E24	1	2	—	Harbor Res
F25	1	2	—	Wave Group
F26	1	2	—	Wave Group
F27	1	2	—	Wave Group
F28	1	2	—	Wave Group

Note: Gage layouts consist of 8 gages.

**Appendix B-2  
Reflective Phase Run Numbers, Harbor Idealized Tests**

Test Case	Gage Layout					Wave Condition
	1	2	3	4	5	
A01	6	—	—	—	—	Regular
A02	5	6	7	8	9	Regular
A03	4	5	6	7	8	Regular
A04	4	—	—	—	—	Regular
A05	4	5	6	7	8	Regular
A06	4	5	6	7	8	Regular
A07	4	5	6	7	8	Regular
A08	4	5	6	7	8	Regular
B01	3	4	5	6	7	Irregular
B02	3	4	5	6	7	Irregular
C01	3	4	5	6	7	Irregular
C02	3	4	5	6	7	Irregular
D01	3	4	5	6	7	Irregular
D02	3	4	5	6	7	Irregular
E21	3	4	5	6	7	Harbor Res
E22	3	4	5	6	7	Harbor Res
E23	3	4	5	6	7	Harbor Res
E24	3	4	5	6	7	Harbor Res
F25	3	4	5	6	7	Wave Group
F26	3	4	5	6	7	Wave Group
F27	3	4	5	6	7	Wave Group
F28	3	—	—	—	—	Wave Group
G02	1	2	—	—	—	Channel Ent
G03	1	2	—	—	—	Channel Ent
G05	1	2	—	—	—	Channel Ent
G06	1	2	—	—	—	Channel Ent
G07	1	2	—	—	—	Channel Ent
G08	1	2	—	—	—	Channel Ent

Note: Gage layouts consist of 20 gages.

**Appendix B-3  
Low-Reflective Phase Run Numbers, Harbor Idealized Tests**

Test Case	Gage Layout					Wave Condition
	1	2	3	4	5	
A02	13	14	12	11	10	Regular
A03	12	13	11	10	9	Regular
A05	12	13	11	10	9	Regular
A06	12	13	11	10	9	Regular
A07	12	13	11	10	9	Regular
A08	12	13	11	10	9	Regular
B01	11	12	10	9	8	Irregular
B02	11	12	10	9	8	Irregular
C01	11	12	10	9	8	Irregular
C02	11	12	10	9	8	Irregular
D01	11	12	10	9	8	Irregular
D02	11	12	10	9	8	Irregular
E21	11	12	10	9	8	Harbor Res
E22	11	12	10	9	8	Harbor Res
E23	11	12	10	9	8	Harbor Res
E24	11	12	10	9	8	Harbor Res
F25	11	12	10	9	8	Wave Group
F26	11	12	10	9	8	Wave Group
F27	11	12	10	9	8	Wave Group
F28	—	—	—	—	—	Wave Group
G02	3	4	—	—	—	Channel Ent
G03	3	4	—	—	—	Channel Ent
G05	3	4	—	—	—	Channel Ent
G06	3	4	—	—	—	Channel Ent
G07	3	4	—	—	—	Channel Ent
G08	3	4	—	—	—	Channel Ent

Note: Gage layouts consist of 20 gages.

**Appendix B-4  
Wave-Current Phase Run Numbers, Wave Gages Only  
Harbor Idealized Tests**

Test Case	Gage Layout 1		Wave Condition
	Wave Only	Wave/Current	
A02	15	16	Regular
A03	14	15	Regular
A05	14	15	Regular
A06	14	15	Regular
A07	14	15	Regular
A08	14	15	Regular
B01	13	14	Irregular
B02	13	14	Irregular
C01	13	14	Irregular
C02	13	14	Irregular
D01	13	14	Irregular
D02	13	14	Irregular

Note: Gage layout consists of 20 gages.

**Appendix B-5  
Wave-Current Phase Run Numbers, Current Meters Only  
Harbor Idealized Tests**

Test Case	Gage Layout 2 Subsets						Wave/Current Condition
	a	b	c	d	e	f	
<b>CURRENT</b>	1	2	3	4	5	6	<b>Currents</b>
A02	17	18	19	20	21	22	Regular
A03	16	17	18	19	20	21	Regular
A05	16	17	18	19	20	21	Regular
A06	16	17	18	19	20	21	Regular
A07	16	17	18	19	20	21	Regular
A08	16	17	18	19	20	21	Regular
B01	15	16	17	18	19	20	Irregular
B02	15	16	17	18	19	20	Irregular
C01	15	16	17	18	19	20	Irregular
C02	15	16	17	18	19	20	Irregular
D01	15	16	17	18	19	20	Irregular
D02	15	16	17	18	19	20	Irregular

**Note:** Gage layout consists of 4 current meters moved through 20 gage locations.  
 Location 2a includes current meters 16-19.  
 Location 2b includes current meters 6-8 and 20.  
 Location 2c includes current meters 9-12.  
 Location 2d includes current meters 13, 15, and 5 (14 bad).  
 Location 2e includes current meters 14, 3 and 4.  
 Location 2f includes current meters 1-4 (3 and 4 re-run).

# **Appendix C Gage Coordinates**

---

**Appendix C-1  
Global System Gage Location Coordinates, Harbor Idealized Tests**

Gage No.	Gage Layout									
	1		2		3		4		5	
	X	Y	X	Y	X	Y	X	Y	X	Y
<b>Calibration Phase</b>										
1	50.83	19.42	50.83	19.42	50.83	19.42				
2	87.33	21.42	15.96	75.54	15.96	75.54				
3	50.83	21.42	50.83	21.42	50.83	21.42				
4	73.33	21.42	22.82	104.47	73.33	21.42				
5	71.33	21.42	17.47	101.56	71.33	21.42				
6	65.33	21.42	13.88	99.61	65.33	21.42				
7	61.33	21.42	6.78	95.75	61.33	21.42				
8	50.83	26.42	50.83	26.42	50.83	26.42				
<b>Reflective Phase</b>										
1	73.33	21.42	73.33	21.42	73.33	21.42	73.33	21.42	73.33	21.42
2	73.33	37.42	73.33	37.42	73.33	37.42	73.33	37.42	73.33	37.42
3	78.44	58.37	1.33	97.10	3.11	98.01	11.11	79.03	37.81	14.61
4	76.24	58.37	1.80	96.22	3.59	97.13	11.59	78.15	38.68	115.09
5	74.04	58.37	2.28	95.34	4.07	96.25	12.07	77.28	39.56	115.56
6	71.84	58.37	2.76	94.46	4.54	95.37	12.55	76.40	40.44	116.04
7	69.64	58.37	3.24	93.58	5.02	94.49	13.02	75.52	41.32	116.52
8	67.44	58.37	3.71	92.70	5.50	93.61	13.50	74.64	42.20	117.00
9	78.44	66.37	4.19	91.83	5.98	92.73	13.98	73.76	43.07	117.48
10	76.24	66.37	4.67	90.95	6.45	91.86	14.46	72.88	43.95	117.96
11	74.04	66.37	5.15	90.07	6.93	90.98	14.93	72.00	44.83	118.44
12	71.84	66.37	5.60	89.19	7.40	90.11	15.40	71.12	45.71	118.92
13	69.64	66.37	6.08	88.31	7.88	89.24	15.88	70.24	46.59	119.40
14	67.44	66.37	6.55	87.43	8.35	88.37	16.35	69.36	47.47	119.88
15	74.13	74.37	58.81	82.37	6.30	96.32	14.30	77.35	39.49	117.80
16	71.93	74.37	61.01	82.37	6.78	95.45	14.78	76.47	40.37	118.28
17	69.73	74.37	63.21	82.37	7.26	94.57	15.26	75.60	41.25	118.76
18	67.53	74.37	65.41	82.37	7.73	93.69	15.74	74.72	42.12	119.24
19	65.33	74.37	67.61	82.37	8.21	92.81	16.21	73.84	43.00	119.72
20	63.13	74.37	69.81	82.37	8.69	91.93	16.69	72.96	43.88	120.20

**Appendix C-2  
Global System Gage Location Coordinates, Harbor Idealized Tests**

Gage No.	Gage Layout									
	1		2		3		4		5	
	X	Y	X	Y	X	Y	X	Y	X	Y
<b>Low-Reflective Phase</b>										
1	73.33	21.42	73.33	21.42	73.33	21.42	73.33	21.42	73.33	21.42
2	73.33	37.42	73.33	37.42	73.33	37.42	73.33	37.42	73.33	37.42
3	78.40	58.37	4.07	96.24	5.83	97.20	11.92	81.76	38.76	112.86
4	76.20	58.37	4.54	95.36	6.30	96.32	12.39	80.88	39.64	113.34
5	74.00	58.37	5.02	94.48	6.78	95.44	12.87	80.00	40.52	113.82
6	71.80	58.37	5.50	93.60	7.26	94.56	13.35	79.13	41.40	114.30
7	69.60	58.37	5.97	92.73	7.73	93.68	13.82	78.25	42.28	114.78
8	67.40	58.37	6.45	91.85	8.21	92.80	14.30	77.37	43.16	115.25
9	78.40	66.37	6.93	90.97	8.68	91.92	14.78	76.49	44.03	115.73
10	76.20	66.37	7.40	90.09	9.16	91.04	15.25	75.61	44.91	116.21
11	74.00	66.37	7.88	89.21	9.64	90.16	15.73	74.73	45.79	116.69
12	71.80	66.37	9.34	99.10	7.58	98.15	13.67	82.72	37.81	114.63
13	69.60	66.37	9.82	98.22	8.06	97.27	14.15	81.84	38.69	115.10
14	67.44	66.37	10.30	97.34	8.54	96.39	14.63	80.96	39.57	115.58
15	74.13	74.37	58.81	82.37	9.01	95.51	15.10	80.08	40.44	116.06
16	71.93	74.37	61.01	82.37	9.49	94.63	15.58	79.20	41.32	116.54
17	69.73	74.37	63.21	82.37	9.97	93.75	16.06	78.32	42.20	117.02
18	67.53	74.37	65.41	82.37	10.44	92.87	16.53	77.44	43.08	117.49
19	65.33	74.37	67.61	82.37	10.92	91.99	17.01	76.56	43.96	117.97
20	63.13	74.37	69.81	82.37	11.40	91.12	17.49	75.68	44.84	118.45

(Continued)

**Appendix C-2 (Concluded)**

Gage No.	Gage Layout									
	1		2		3		4		5	
	X	Y	X	Y	X	Y	X	Y	X	Y
Wave-Current Phase										
1	78.43	34.67	78.43	34.67						
2	83.43	34.67	83.43	34.67						
3	88.43	34.67	88.43	34.67						
4	93.43	34.67	93.43	34.67						
5	98.43	34.67	98.43	34.67						
6	70.96	46.67	70.96	46.67						
7	73.16	46.67	73.16	46.67						
8	75.36	46.67	75.36	46.67						
9	77.56	46.67	77.56	46.67						
10	79.76	46.67	79.76	46.67						
11	81.96	46.67	81.96	46.67						
12	84.16	46.67	84.16	46.67						
13	86.36	46.67	86.36	46.67						
14	88.56	46.67	88.56	46.67						
15	90.76	46.67	90.76	46.67						
16	85.49	58.67	65.49	58.67						
17	80.49	58.67	70.49	58.67						
18	75.49	58.67	75.49	53.67						
19	70.49	58.67	80.49	58.67						
20	65.49	58.67	85.49	58.67						

**Appendix C-3  
Numerical Model X"/Y" Gage Location Coordinates, Harbor Idealized Tests**

Gage No.	Gage Layout									
	1		2		3		4		5	
	X	Y	X	Y	X	Y	X	Y	X	Y
<b>Calibration Phase</b>										
1	73.78	50.83	73.78	50.83	73.78	50.83				
2	71.78	87.33	17.66	15.96	17.66	15.96				
3	71.78	50.83	71.78	50.83	71.78	50.83				
4	71.78	73.33	-11.27	22.82	71.78	73.33				
5	71.78	71.33	-8.36	17.47	71.78	71.33				
6	71.78	65.33	-6.41	13.88	71.78	65.33				
7	71.78	61.33	-2.55	6.78	71.78	61.33				
8	66.78	50.83	66.78	50.83	66.78	50.83				
<b>Reflective Phase</b>										
1	71.78	73.33	71.78	73.33	71.78	73.33	71.78	73.33	71.78	73.33
2	55.78	73.33	55.78	73.33	55.78	73.33	55.78	73.33	55.78	73.33
3	34.83	78.44	-3.90	1.33	-4.81	3.11	14.17	11.11	78.59	37.81
4	34.83	76.24	-3.02	1.80	-3.93	3.59	15.05	11.59	-21.89	38.68
5	34.83	74.04	-2.14	2.28	-3.05	4.07	15.92	12.07	-22.36	39.56
6	34.83	71.84	-1.26	2.76	-2.17	4.54	16.80	12.55	-22.84	40.44
7	34.83	69.64	-0.38	3.24	-1.29	5.02	17.68	13.02	-23.32	41.32
8	34.83	67.44	0.50	3.71	-0.41	5.50	18.56	13.50	-23.80	42.20
9	26.83	78.44	1.37	4.19	0.47	5.98	19.44	13.98	-24.28	43.07
10	26.83	76.24	2.25	4.67	1.34	6.45	20.32	14.46	-24.76	43.95
11	26.83	74.04	3.13	5.15	2.22	6.93	21.20	14.93	-25.24	44.83
12	26.83	71.84	-6.76	6.60	-5.76	4.87	13.21	12.87	-23.17	36.86
13	26.83	69.64	-5.88	7.08	-4.88	5.35	14.09	13.35	-23.65	37.73
14	26.83	67.44	-5.00	7.55	-4.00	5.82	14.97	13.83	-24.13	38.61
15	18.83	74.13	10.83	58.81	-3.12	6.30	15.85	14.30	-24.60	39.49
16	18.83	71.93	10.83	61.01	-2.25	6.78	16.73	14.78	-25.08	40.37
17	18.83	69.73	10.83	63.21	-1.37	7.26	17.60	15.26	-25.56	41.25
18	18.83	67.53	10.83	65.41	-0.49	7.73	18.48	15.74	-26.04	42.12
19	18.83	65.33	10.83	67.61	0.39	8.21	19.36	16.21	-26.52	43.00
20	18.83	63.13	10.83	69.81	1.27	8.69	20.24	16.69	-27.00	43.88

**Appendix C-4  
Numerical Model X"/Y" Gage Location Coordinates, Harbor Idealized Tests**

Gage No.	Gage Layout									
	1		2		3		4		5	
	X	Y	X	Y	X	Y	X	Y	X	Y
<b>Low-Reflective Phase</b>										
1	71.78	73.33	71.78	73.33	71.78	73.33	71.78	73.33	71.78	73.33
2	55.78	73.33	55.78	73.33	55.78	73.33	55.78	73.33	55.78	73.33
3	34.83	78.40	-3.04	4.07	-4.00	5.83	11.44	11.92	-19.66	38.76
4	34.83	76.20	-2.16	4.54	-3.12	6.30	12.32	12.39	-20.14	39.64
5	34.83	74.00	-1.28	5.02	-2.24	6.78	13.20	12.87	-20.62	40.52
6	34.83	71.80	-0.40	5.50	-1.36	7.26	14.07	13.35	-21.10	41.40
7	34.83	69.60	0.47	5.97	-0.48	7.73	14.95	13.82	-21.58	42.28
8	34.83	67.40	1.35	6.45	0.40	8.21	15.83	14.30	-22.05	43.16
9	26.83	78.40	2.23	6.93	1.28	8.68	16.71	14.78	-22.53	44.03
10	26.83	76.20	3.11	7.40	2.16	9.16	17.59	15.25	-23.01	44.91
11	26.83	74.00	3.99	7.88	3.04	9.64	18.47	15.73	-23.49	45.79
12	26.83	71.80	-5.90	9.34	-4.95	7.58	10.48	13.67	-21.43	37.81
13	26.83	69.60	-5.02	9.82	-4.07	8.06	11.36	14.15	-21.90	38.69
14	26.83	67.44	-4.14	10.30	-3.19	8.54	12.24	14.63	-22.38	39.57
15	18.83	74.13	10.83	58.81	-2.31	9.01	13.12	15.10	-22.86	40.44
16	18.83	71.93	10.83	61.01	-1.43	9.49	14.00	15.58	-23.34	41.32
17	18.83	69.73	10.83	63.21	-0.55	9.97	14.88	16.06	-23.82	42.20
18	18.83	67.53	10.83	65.41	0.33	10.44	15.76	16.53	-24.29	43.08
19	18.83	65.33	10.83	67.61	1.21	10.92	16.64	17.01	-24.77	43.96
20	18.83	63.13	10.83	69.81	2.08	11.40	17.52	17.49	-25.25	44.84

(Continued)

<b>Appendix C-4 (Concluded)</b>										
<b>Gage No.</b>	<b>Gage Layout</b>									
	<b>1</b>		<b>2</b>		<b>3</b>		<b>4</b>		<b>5</b>	
	<b>X</b>	<b>Y</b>	<b>X</b>	<b>Y</b>	<b>X</b>	<b>Y</b>	<b>X</b>	<b>Y</b>	<b>X</b>	<b>Y</b>
<b>Wave-Current Phase</b>										
1	58.53	78.43	58.53	78.43						
2	58.53	83.43	58.53	83.43						
3	58.53	88.43	58.53	88.43						
4	58.53	93.43	58.53	93.43						
5	58.53	98.43	58.53	98.43						
6	46.53	70.96	46.53	70.96						
7	46.53	73.16	46.53	73.16						
8	46.53	75.36	46.53	75.36						
9	46.53	77.56	46.53	77.56						
10	46.53	79.76	46.53	79.76						
11	46.53	81.96	46.53	81.96						
12	46.53	84.16	46.53	84.16						
13	46.53	86.36	46.53	86.36						
14	46.53	88.56	46.53	88.56						
15	46.53	90.76	46.53	90.76						
16	34.53	85.49	34.53	65.49						
17	34.53	80.49	34.53	70.49						
18	34.53	75.49	34.53	75.49						
19	34.53	70.49	34.53	80.49						
20	34.53	65.49	34.53	85.49						

# REPORT DOCUMENTATION PAGE

Form Approved  
OMB No. 0704-0188

Public reporting burden for this collection of information is estimated to average 1 hour per response, including the time for reviewing instructions, searching existing data sources, gathering and maintaining the data needed, and completing and reviewing the collection of information. Send comments regarding this burden estimate or any other aspect of this collection of information, including suggestions for reducing this burden, to Washington Headquarters Services, Directorate for Information Operations and Reports, 1215 Jefferson Davis Highway, Suite 1204, Arlington, VA 22202-4302, and to the Office of Management and Budget, Paperwork Reduction Project (0704-0188), Washington, DC 20503

<b>1. AGENCY USE ONLY (Leave blank)</b>	<b>2. REPORT DATE</b> March 1993	<b>3. REPORT TYPE AND DATES COVERED</b> Final report	
<b>4. TITLE AND SUBTITLE</b> Laboratory Description of Harbor Idealized Tests; Volume I: Main Text and Appendixes A Through C; Volume II: Appendix D		<b>5. FUNDING NUMBERS</b>	
<b>6. AUTHOR(S)</b> Michael J. Briggs, Edward F. Thompson, Debra R. Green, Linda S. Lillycrop		<b>8. PERFORMING ORGANIZATION REPORT NUMBER</b>  Technical Report CERC-93-1	
<b>7. PERFORMING ORGANIZATION NAME(S) AND ADDRESS(ES)</b> U.S. Army Engineer Waterways Experiment Station Coastal Engineering Research Center 3909 Halls Ferry Road, Vicksburg, MS 39180-6199		<b>10. SPONSORING/MONITORING AGENCY REPORT NUMBER</b>	
<b>9. SPONSORING/MONITORING AGENCY NAME(S) AND ADDRESS(ES)</b> U.S. Army Corps of Engineers Washington, DC 20314-1000		<b>11. SUPPLEMENTARY NOTES</b>  Available from National Technical Information Service, 5285 Port Royal Road, Springfield, VA 22161.	
<b>12a. DISTRIBUTION/AVAILABILITY STATEMENT</b> Approved for public release; distribution is unlimited.		<b>12b. DISTRIBUTION CODE</b>	
<b>13. ABSTRACT (Maximum 200 words)</b>  A three-dimensional, physical model study of a generalized harbor and entrance using regular and irregular waves and tidal ebb currents was conducted in the directional spectral wave basin. The purpose of this study was to (a) gain a better understanding of the physics involved in wave transformation from deep water into harbors, (b) confirm accurate simulation of this transformation in physical models, (c) verify the HARBD numerical model, a steady-state hybrid element model which includes the effects of bottom friction and boundary absorption in harbors of arbitrary configuration and variable bathymetry, and (d) generate a data set for improving Corps design procedures. The three-dimensional, 1:45 scale physical model reproduced a rectangular, 40-ft-deep flat-bottom harbor, contoured 40-ft entrance channel, and nearshore bathymetry. Bathymetry of the entrance channel and offshore area were representative of field conditions.  The physical model of the idealized harbor included regular and irregular waves and ebb currents to study the effects that frequency and directional spreading, harbor resonance, wave grouping, channel entrance, and wave-current interaction have on harbor response. Typical prototype wave periods were 8 and 14 sec (1.19  <div style="text-align: right;">(Continued)</div>			
<b>14. SUBJECT TERMS</b> Data sets Harbor modeling Harbor numerical models		Harbor wave transformation Irregular waves Physical models	
<b>17. SECURITY CLASSIFICATION OF REPORT</b> UNCLASSIFIED		<b>15. NUMBER OF PAGES</b> Vol I-87; Vol II-307	
<b>18. SECURITY CLASSIFICATION OF THIS PAGE</b> UNCLASSIFIED		<b>16. PRICE CODE</b>	
<b>19. SECURITY CLASSIFICATION OF ABSTRACT</b>		<b>20. LIMITATION OF ABSTRACT</b>	

13. (Concluded).

and 2.09 sec, respectively, in the model). A prototype wave height of 3.75 ft (1 in. model) was selected for all tests to prevent overtopping and breaking and minimize nonlinear interactions. Waves had overall mean wave directions of 0 deg and  $\pm 22.5$  deg, relative to a direction perpendicular to the wavemaker. Tidal ebb currents of 0.5 knot (0.88 fps prototype, 0.13 fps model) were created to study the wave-current interaction in the nearshore region outside the entrance channel. Boundary conditions in the harbor and channel included fully reflecting vertical walls and low-reflecting 1:1.3 revetted stone slopes. A total of 374 runs were completed using 20 capacitance wave gages and 4 electromagnetic current meters in 9 different gage configurations. Gage locations were selected near the basin boundaries (i.e. corners), the areas where the largest harbor response is typically observed.

This report describes the laboratory data collection effort and documents model set-up, wave conditions, the test program, and the testing procedure.